Click Here for Full Article

Neogene uplift of the Tian Shan Mountains observed in the magnetic record of the Jingou River section (northwest China)

Julien Charreau,[1,2] Yan Chen,[1] Stuart Gilder,[3] Laurie Barrier,[4] Stéphane Dominguez,[5] Romain Augier,[1] Sevket Sen,[6] Jean-Philippe Avouac,[7] Audrey Gallaud,[1] Fabien Graveleau,[5] and Qingchen Wang[8]

Received 27 March 2008; revised 25 June 2008; accepted 15 December 2008; published 31 March 2009.

[1] The Tian Shan Mountains constitute central Asia's longest and highest mountain range. Understanding their Cenozoic uplift history thus bears on mountain building processes in general, and on how deformation has occurred under the influence of the India-Asia collision in particular. In order to help decipher the uplift history of the Tian Shan, we collected 970 samples for magnetostratigraphic analysis along a 4571-m-thick section at the Jingou River (Xinjiang Province, China). Stepwise alternating field and thermal demagnetization isolate a linear magnetization component that is interpreted as primary. From this component, a magnetostratigraphic column composed of 67 polarity chrons are correlated with the reference geomagnetic polarity timescale between ~1 Ma and ~23.6 Ma, with some uncertainty below ~21 Ma. This correlation places precise temporal control on the Neogene stratigraphy of the southern Junggar Basin and provides evidence for two significant stepwise increases in sediment accumulation rate at ~16–15 Ma and ~11–10 Ma. Rock magnetic parameters also undergo important changes at ~16–15 Ma and ~11–10 Ma that correlate with changes in sedimentary depositional environments. Together with previous work, we conclude that growth history of the modern Tian Shan Mountains includes two pulses of uplift and erosion at ~16–15 Ma and ~11–10 Ma. Middle to upper Tertiary rocks around the Tian Shan record very young (<~5 Ma) counterclockwise paleomagnetic rotations, on the order of 15° to 20°, which are interpreted as because of strain partitioning with a component of sinistral shear that localized rotations in the piedmont. **Citation:** Charreau, J., et al. (2009), Neogene uplift of the Tian Shan Mountains observed in the magnetic record of the Jingou River section (northwest China), *Tectonics*, *28*, TC2008, doi:10.1029/2007TC002137.

1. Introduction

[2] Significant progress has been made over the past few decades to understand how the Asian continent was built under the influence of the India-Asia collision. Most ideas fall within two end-member models that range from discontinuous deformation and extrusion along prescribed faults [e.g., *Tapponnier and Molnar*, 1976; *Peltzer et al.*, 1982] to a continuum style of large-scale deformation [e.g., *England and Houseman*, 1986; *England and Molnar*, 1997]. Defining where and when deformation occurred is essential to solve the tectonic history of this vast region, which also holds important constraints on climate change and species evolution and migration patterns [e.g., *Rage et al.*, 1995; *Jaeger et al.*, 1989]. Although the onset of the India-Asia collision at ~55 Ma [e.g., *Patriat and Achache*, 1984] is relatively well accepted, with notable exceptions [e.g., *Aitchison et al.*, 2002], large uncertainties surround the timing of the deformation that generated the high topography associated with the collision. Some models argue that mountain building propagated northward [*Molnar et al.*, 1993; *Métivier and Gaudemer*, 1997; *Tapponnier et al.*, 2001] leading to younger uplift to the north, while others find evidence for a more sporadic evolution in time and place [*Avouac and Tapponnier*, 1992; *Chen et al.*, 2002].

[3] The Tian Shan Mountains lie around 1700 km north of the suture that demarcates the boundary between the Indian and Asian plates. Despite the distance from the Indian indenter, this 2500 east-west trending range dominates the central Asian landscape with summits higher than 7000 m (Podeby Peak, 7439 m). Shortening rates exceeding 20 mm/a across the range [*Abdrakhmatov et al.*, 1996; *Reigber et al.*, 2001] attest to a high rate of intracontinental deformation and account for about 40% of the total India-Asia convergence being absorbed within the Tian Shan. Thus, understanding how and when these mountains were built will not only improve our knowledge of mountain building processes in general, but how deformation has acted to form the vast area under the influence of the India-Asia collision.

[1]Institut des Sciences de la Terre d'Orléans, Orléans, France.
[2]Now at Centre de Recherches Pétrographiques et Géochimiques, Vandoeuvre-lès-Nancy, France.
[3]Geophysics Section, Department of Earth and Environmental Sciences, Ludwig Maximilians University, Munich, Germany.
[4]Institut de Physique du Globe de Paris, Paris, France.
[5]Géosciences Montpellier, UMR 5243, UMII, Université Montpellier 2, CNRS, Montpellier, France.
[6]Museum of Natural History, UMR 5143, Paléobiodiversité et Paléoenvironnements, CNRS, Paris, France.
[7]Tectonics Observatory, California Institute of Technology, Pasadena, California, USA.
[8]State Key Laboratory of Lithospheric Evolution, Institute of Geology and Geophysics, Chinese Academy of Sciences, Beijing, China.

Copyright 2009 by the American Geophysical Union.
0278-7407/09/2007TC002137$12.00

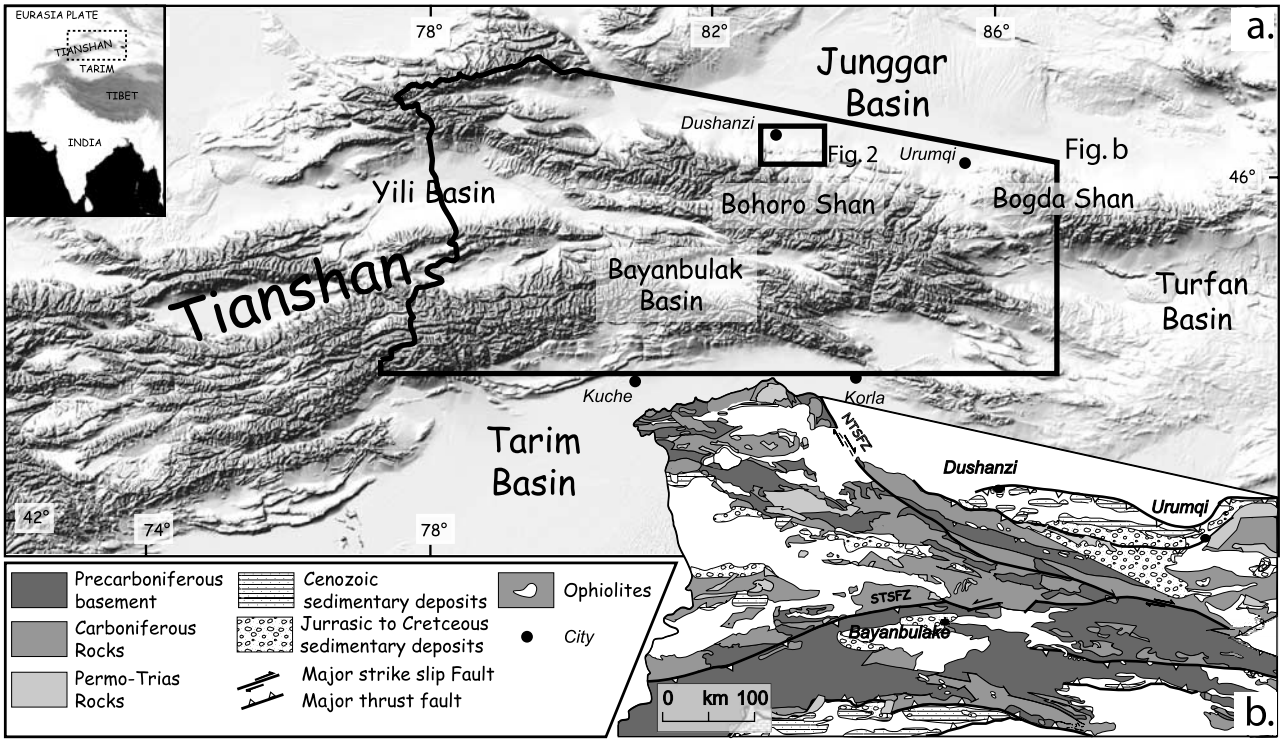

Figure 1. (a) Topographic map of central Asia. (b) Geological map of the Tian Shan area. NTSFZ, North Tian Shan Fault Zone; STSFZ, South Tian Shan Fault Zone.

[4] The geologic history of the Tian Shan may be traced back to the Paleozoic with the accretion of island arc terrains in the Devonian to Carboniferous [e.g., *Burtman*, 1975; *Windley et al.*, 1990]. Despite the absence of significant exhumation, the Tian Shan Mountains probably remained higher than their surroundings during the Mesozoic [*Hendrix et al.*, 1992]. Although most workers conclude that a significant uplift event occurred during the middle to late Cenozoic, there lacks a general agreement as to the precise timing. Much of the differences lie in the method of observation, with ages ranging from the late Oligocene [*Windley et al.*, 1990; *Hendrix et al.*, 1994; *Dumitru et al.*, 2001; *Heermance et al.*, 2007] to the middle to late Miocene [*Avouac et al.*, 1993, *Abdrakhmatov et al.*, 1996; *Métivier and Gaudemer*, 1997; *Bullen et al.*, 2001; *Charreau et al.*, 2006] and even in the latest Cenozoic or Quaternary [e.g., *Burchfiel et al.*, 1999].

[5] Fission track dating of in situ apatite from Mesozoic sandstone located in the northern piedmont led *Hendrix et al.* [1992] to place the initiation of Tian Shan uplift at about 24 Ma. Thermal modeling by *Dumitru et al.* [2001] on detrital and magmatic apatite along the Dushanzi/Kuche transect (Figure 1) suggest that the Tian Shan underwent two main phases of exhumation in the Late Paleozoic and the late Cenozoic. *Dumitru et al.* [2001] argued that the faults along the northern flank of the Tian Shan accommodated shortening and exhumation since at least 25 Ma. However, combining U-Th/He thermochronology with magnetostratigraphy at the Chu basin (western Tian Shan), *Bullen et al.* [2001, 2003] argued that the western Kyrgyz range underwent a rapid exhumation beginning at ~11 Ma. *Sobel et al.* [2006] came to a similar conclusion by analyzing fission tracks from three transects in the Kyrgyz Tian Shan and demonstrated that the range propagated over 110 km eastward over the last ~7–11 Ma.

[6] On the basis of balanced cross sections, *Avouac et al.* [1993] estimated that deformation initiated across the Tian Shan at ca. 15 Ma. Their calculation assumed a constant shortening rate of ~3 mm/a derived from fault scarp analyses along the northern Tian Shan piedmont which is coherent with the total shortening rate observed by GPS at this longitude (5–6 mm/a [*Abdrakhmatov et al.*, 1996; *Reigber et al.*, 2001]). As the timing for the initiation of uplift depends on the shortening rate and how well the rate represents a long-term average, one must question how far the measurements can be linearly extrapolated back in time.

[7] Because the Tian Shan are sandwiched between two large intracontinental basins, Junggar to the north and Tarim to the south (Figure 1a), the uplift history of the Tian Shan can potentially be deciphered from sediments eroded from the mountains and deposited in these adjacent basins. Near Urumqi city, for example, *Windley et al.* [1990] observed the deposition of Oligocene conglomerates above an unconformity and interpreted this as the mark of the onset of deformation induced by the India-Asia collision. However, the age of those conglomerates are uncertain. On the basis of drill core logs, *Métivier and Gaudemer* [1997] calculated the mass accumulation rates in the Junggar and Tarim basins and placed the beginning of major uplift at about 16 Ma, with acceleration at 5 Ma that they proposed to coincide with an uplift pulse of the Tian Shan.

[8] A significant change in lithology occurred in both the Junggar and the Tarim basins during the upper Cenozoic. This change coincides with the deposition of a thick conglomerate, called the Xiyu Formation [*Chen et al.*, 1994; *Liu et al.*, 1996; *Zheng et al.*, 2000], over Neogene sediments [*Burchfiel et al.*, 1999; *Fu et al.*, 2003]. The appearance of the Xiyu Formation may mark the time of major uplift of the Tian Shan. However, their deposition was more likely diachronous in space and time [e.g., *Charreau et al.*, 2005]. Moreover, thick piles of conglomerates are recognized throughout central Asia and the Tibetan Plateau, which has led other workers to propose that their deposition is more related to climate change than to tectonism [*Molnar and England*, 1990; *Liu et al.*, 1996; *Zhang et al.*, 2001; *Molnar*, 2004].

[9] Using the stratigraphic record to understand the Cenozoic uplift history of the Tian Shan Mountains has a serious drawback: the continental facies sediments are fossil poor and lack volcanic horizons, which imposes large age uncertainties. This makes magnetostratigraphy the technique of choice to date the deposits. Magnetostratigraphy provides a continuous, high-resolution time record of the sediments whose detailed sediment accumulation rates can be used to reconstruct the erosion history of the range. Moreover, by studying variations in magnetic mineralogy and sedimentary fabric through time, one can trace potential changes in source rock and/or the hydrodynamic regime acting during erosion, transport and sedimentation. These will in turn reflect the tectonic and/or climatic environment acting on the Tian Shan. To this aim, we carried out two magnetostratigraphic and rock magnetic studies on Neogene sediments exposed on both flanks of the Tian Shan at approximately the same longitude. At the Kuitun section (Junggar basin, northern Tian Shan; Figure 1), we found that sediment accumulation rates and rock magnetic characteristics of the sediments remained relatively constant from ~10.5 Ma to ~3.1 Ma [*Charreau et al.*, 2005] [see also *Sun et al.*, 2007; *Charreau et al.*, 2008a]. This led us to argue that exhumation at Kuitun commenced before ~10.5 Ma. At the Yaha section (Tarim basin, southern Tian Shan, Figure 1) we identified a twofold increase in sedimentation rate at ~11 Ma that coincided with important changes in the rock magnetic characteristics of the sediments [*Charreau et al.*, 2006]. This led us to confer with the conclusions of *Bullen et al.* [2001] that the Tian Shan underwent an important phase of uplift and erosion at ~11 Ma. Findings by *Sobel et al.* [2006] lend support to this conclusion. About 10 km from the Yaha section, *Huang et al.* [2006] identified uplift pulses at ~20 Ma and at ~16–17 Ma from a magnetostratigraphic study, while conclusions regarding the younger part of the section are under debate [*Charreau et al.*, 2008b].

[10] Because the oldest sediments sampled at the Kuitun section were ~10.5 Ma, robust conclusions could not be drawn as to when that segment of the northern Tian Shan became active other than it must have been prior to ~10.5 Ma. We thus searched for another section on the northern flank of the Tian Shan that potentially spanned farther back in time. A suitable section was found ~70 km east of Kuitun, along the Jingou River, south of where it intersects the Anjihai River (Figures 1 and 2). Below we present the magnetostratigraphy, rock magnetism and a preliminary sedimentary analysis of the Jingou River section. The results are then discussed in a broader context of the Cenozoic uplift and erosion history of the Tian Shan Mountains.

2. Geological Setting and Sampling

[11] The northern Tian Shan piedmont extends about 240 km, between the cities of Urumqi and Dushanzi (Figure 1a). It consists of three main fold and thrust fault belts, which are mainly fault-bend folds and detachment folds that deformed strata from the south Junggar basin. The Junggar basin is a typical foreland basin that was continuously filled by sediments shed from the Tian Shan from Permian to Quaternary times (see, for example, paleocurrent analysis of *Hendrix et al.* [1992]). During Cenozoic time, no major deposition gap (discontinuity or unconformity) exists that could mark the onset of Tian Shan uplift reactivation. Fold belts are well exposed along north flowing rivers that cut the piedmont, likely during the Holocene [e.g., *Poisson and Avouac*, 2004]. Close to Shawan city, the Jingou River incises the Huo'erguosi fault bend-fold anticline in the hanging wall of a north verging thrust (Figure 2c) to expose a continuous outcrop of south dipping sediments that we sampled for our study.

[12] The Jingou River section comprises five formations described in the Chinese literature [e.g., *Bureau of Geological and Mineral Resources of the Xinjiang Uygur Autonomous Region* [BGMRX, 1993] which are from bottom to top, the Anjihaihe, Shawan, Taxihe, Dushanzi and Xiyu formations (Figure 2c). All these formations are well exposed in the southern limb of the Huo'erguosi anticline and are thrust over Cenozoic sediments and a Quaternary terrace to the north, which implies that the faulting is still active. The start of faulting and folding might be a bit older during late Pliocene because of the presence of growth strata in the southern limb of the Huo'erguosi anticline [*Molnar et al.*, 1994; *Burchfiel et al.*, 1999].

[13] The Anjihaihe Formation crops out at the northernmost part of the section. Our sampling began at the top of this formation that is, as described by *BGMRX* [1993], composed of upper Paleogene green mudstones to sandstones. The overlying Shawan Formation, mapped as Neogene [*BGMRX*, 1993], contains dark red mudstones to muddy sandstones intercalated with argillaceous beds and gray conglomerates [*BGMRX*, 1993]. To the south, the Shawan Formation is overlain by the Taxi He Formation, the latter being composed of red to brown mudstones to sandstones intercalated with green sandstones toward its base and green sandstones to mudstones toward the top [*BGMRX*, 1993]. The Dushanzi Formation conformably overlies the Taxi He Formation. Red to brown sandy mudstones and thin argillaceous beds dominate the base of the Dushanzi Formation. The series becomes progressively coarser grained (sandstone and microconglomerate) toward the top as the color grades into shades of brown and yellow with increasing intervals of gray conglomerate. At the Jingou River section, the Dushanzi Formation grades into the overlying Xiyu Formation, but no strict limit between

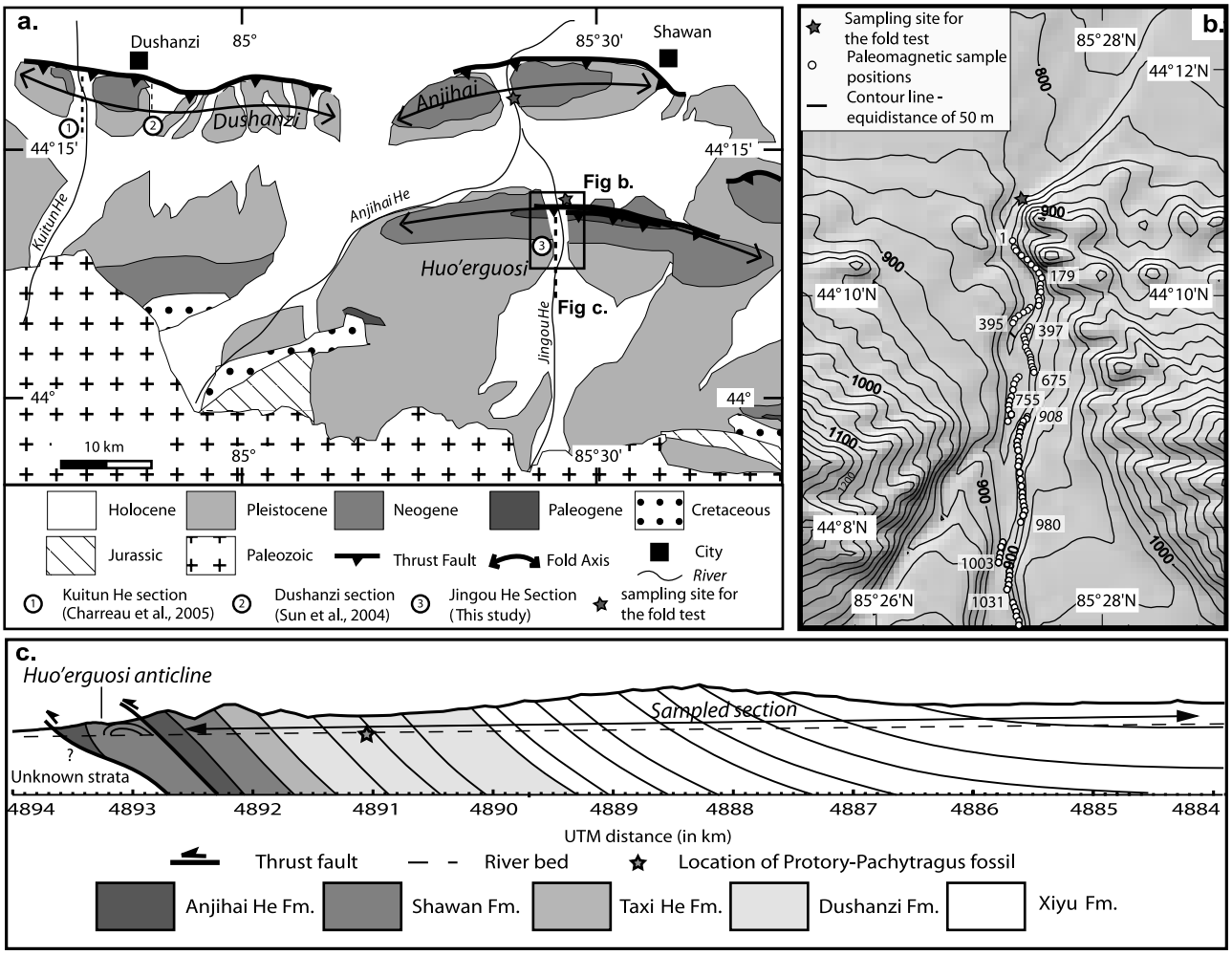

Figure 2. (a) Geological map of the Shawan area [after *Avouac et al.*, 1993] showing the location of the Kuitun section [*Charreau et al.*, 2005], the Dushanzi section [*Sun et al.*, 2004], and the Jingou River magnetostratigraphic section. (b) Detailed topographic map of the Jingou River section with sampling sites. (c) Cross section of the Huo'erguosi anticline indicating the location of the paleomagnetic cores and of *Hypsodontus sp.*

the two is apparent. This formation is widely distributed around central Asia and is composed of dark gray conglomerates that are generally believed to be Plio-Pleistocene in age [e.g., *Chen et al.*, 1994] but may be older in some places [e.g., *Charreau et al.*, 2005] (see section 6.2).

[14] Bedding attitudes are fairly constant along the section with an average strike and dip of N85°E, 55°S. No major fault was identified within the sampled section, meaning that the section was not duplicated. No major discontinuity or unconformity was identified either, suggesting that the sedimentary series is relatively continuous. The magnetostratigraphic section spans 4571 m in thickness with a total of 970 samples composed of 756 drill cores (from 2075 to 4572 m in stratigraphic depth) in the major part of the section and 214 hand samples collected in the upper part of the Dushanzi Formation and the Xiyu Formation (Figure 2). Collecting samples with a gasoline-powered drill was impossible in the conglomerate-rich upper part of the section, so we collected oriented hand samples from fine-grained lenses. When drilling, at least two cores per horizon were collected with an average distance between horizons of 5.5 m. In the upper part where we collected only hand samples, the stratigraphic separation of sample sites is 11.3 m on average. Cores and cubes were oriented using magnetic and, whenever possible, sun compasses. The average magnetic declination anomaly of 3.4° ± 2.4° (N = 183) was used to correct the strike values and the core azimuths lacking sun compass measurements. Bedding attitudes were measured at each sampled horizon; core locations were determined to within a few centimeters using differential GPS. Stratigraphic depth was estimated from the south to the north, 0 starting at the point along the section where bedding attitudes become horizontal assuming

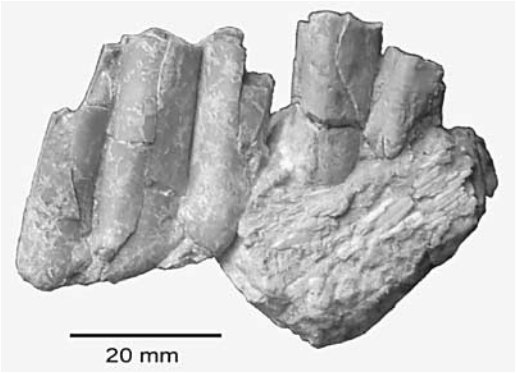

Figure 3. Lower jaw fragment of *Hypsodonthus* sp. with second and third molars in lateral view. Scale bar is 200 mm.

that this corresponds to the original stratigraphic surface. In order to obtain a significant fold test, we drilled 24 samples at three sites on the overturned northern flank of the Huo'erguosi anticline as well as 16 samples at two sites in the Dushanzi Formation along the northern flank of the Anjihai He anticline (Figure 2).

3. Paleontology

[15] At 3165 m in stratigraphic depth, between cores 411 and 413 within the Dushanzi Formation (Figure 2c), we found a lower right jaw with two molars (m2 and m3) belonging to a bovid (Figure 3). The maximum length and width are 19.6 × 10.6 mm and 30.4 × 10.9 mm for m2 and m3, respectively. These teeth have hypsodont crowns; their lingual face is gently folded, and they lack the ectostylid (basal pillar); the third molar has a third rather strong lobe. The hypsodonty index of the less worn third molar is 105. Both teeth are narrow compared to their length. The measurements of the molars are typical of a large sized antelope such as the extant oryx. The size, morphology and strong hypsodonty of these molars suggest a comparison with large middle Miocene genera *Hypsodontus* and *Turkocerus*, and with late Miocene antelopes of the *Protoryx-Pachytragus* group. *Köhler* [1987] studied Neogene bovid from Turkey and revised the systematics of all large-sized antelopes. *Köhler* [1987] grouped their middle Miocene representatives into two genera: *Hypsodontus* [*Sokolov*, 1949] and *Turkocerus* new gen. According to *Köhler* [1987], the difference between these two genera is that *Turkocerus* are smaller species with lower molars having basal pillars, while *Hypsodontus* has larger teeth and lower molars with scarce or absent basal pillars. Another characteristic common to these two genera is that the lower molars, mainly m3, are narrower than in their late Miocene equivalents.

[16] Within the genus *Turkocerus, Köhler* [1987] grouped the two species of antelopes from the Tunggur Formation (Wolf Camp Quarry) in Inner Mongolia that *Pilgrim* [1934] described as *Oioceros*(?) *grangeri* nov. sp. and *Oioceros*(?) *noverca* nov. sp., and a new species from the middle Miocene of Turkey (Çandir), *T. gracilis*. Çandir is dated by magnetostratigraphy at ca 14 Ma while the Wolf Camp Quarry at the Tunggur Formation is dated between 11.5 and 12.4 Ma [*Krijgsman*, 2003; *Wang et al.*, 2003]. In the genus *Hypsodontus, Köhler* [1987] included the type species *H. miocaenicus* [*Sokolov*, 1949] from the early middle Miocene locality of Belometcheskaya (Georgia), *H. serbicus* from the middle Miocene of Prebreza (former Yugoslavia) and a new species *H. pronaticornis* from the middle Miocene localities of Çandir, Pasalar and Yukari Kizilca in Turkey.

[17] Independently, *Chen* [1988] referred *Oioceros*(?) *grangeri* and *Oioceros*(?) *noverca* to the new genera, *Sinomioceros* and *Sinopalaeocerus*, respectively. These are the junior synonyms of *Turkocerus* [*Köhler*, 1987]. On the other hand, *Gabunia* [1973] described a horn core from Belometcheskaya, slightly smaller but with the same pattern, as a new genus and species, *Kubanotragus sokolovi*, and *Chen* [1988] added a new species to this genus, *K. gaopense* from the middle Miocene of Lantian (Shaanxi, China).

[18] Several ruminant specialists have questioned the generic differentiation between all these genera [*Bonis et al.*, 1998; *Gentry et al.*, 1999; *Geraads*, 2003]. They suggested grouping all these large sized middle Miocene antelopes into the genus *Hypsodontus*. Their arguments are the following:

[19] 1. The smaller size of species referred to *Turkocerus* is not reliable since its type species *T. grangeri* from Tunggur is as large as some species of *Hypsodontus*.

[20] 2. The shape of the horns shows both regional and sexual variations when the sample is large enough. In most localities, the material being scarce, one cannot recognize individual and/or specific variations.

[21] 3. Concerning the lower molars, the more frequent occurrence of the basal pillar in *Turkoceros* is not observed in all fossil populations. This structure is often present in some early middle Miocene populations from Turkey and in "*Turkocerus" noverca* from Tunggur, but much less in "*Turkocerus" grangeri* from Tunggur. Concerning genus *Hypsodonthus*, only about 1/4 of its lower molars display a tiny basal pillar.

[22] Large late Miocene antelopes (those being similar in size to that of the Jingou River bovid) are grouped in the genera *Protoryx* and *Pachytragus*. This group is well known in the late Miocene (late Vallesian up to late Turolian) localities of the Aegean area and Middle East, but much less during the late Miocene in East Africa and Central and East Asia. In the recent literature the Asian representative of the group is attributed to the genus *Pachytragus*. In these genera, the lower molars display some degree of hypsodonty like the Jingou River sample, but are proportionally wider than those from the Jingou River. The basal pillar of lower molars may or may not exist from one population to another. *Kostopoulos* [2005] discussed the complicated taxonomy of this group. It appears that generic identification as well species determination needs complete cranial samples. The massive shape of lower molars in the species referred to the *Protoryx Pachytragus* group prevents us to attribute the Jingou River bovid to this group. Taking into account all these observations, we identify this specimen as *Hypsodontus* sp., belonging to the middle Miocene, similar

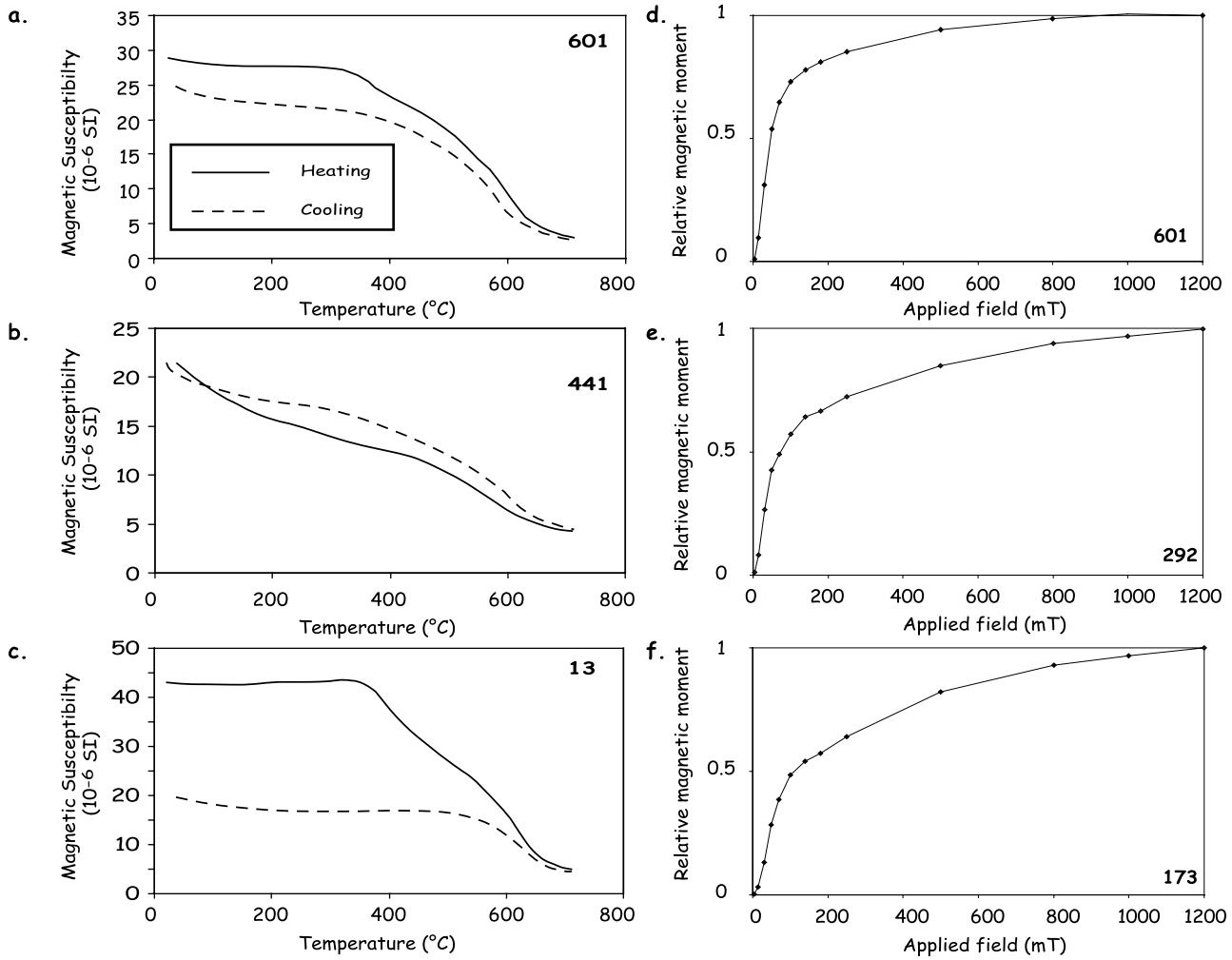

Figure 4. (a, b and c) Curie point analyses and (d, e and f) acquisition of isothermal remanent magnetization of representative samples.

in size to *H. pronaticornis* [*Köhler*, 1987] or "*Turkocerus" grangeri* [*Pilgrim*, 1934].

4. Magnetostratigraphy and Rock Magnetism of the Jingou River Section

4.1. Magnetic Mineralogy

[23] Curie point analyses using an AGICO KLY-3S KappaBridge susceptibility meter coupled with a CS-3 furnace were determined for eight samples distributed along the section. Two deflections in the heating curves were apparent (Figures 4a and 4b): a minor one between 300°C and 400°C that may correspond to maghemite, Ti-rich magnetite or pyrrhotite, and a dominant one at around 580°C that is characteristic of Ti-poor magnetite. A constant decrease in susceptibility above 600°C likely signals the presence of hematite. Most samples displayed fairly reversible heating and cooling curves (Figures 4a and 4b), indicating minor alteration of the magnetic minerals during heating, although a few samples had significantly lower susceptibilities during cooling than during heating (Figure 4c).

[24] Acquisition of isothermal remanent magnetization curves rapidly increase from 0 to 150 mT, with 60 to 70% of the maximum magnetization acquired by ~200 mT for most samples (Figures 4d to 4f). This signals the presence of a magnetic mineral with low coercivity, such as magnetite. The magnetic moment continues to increase above 200 mT and the samples are not saturated by ~1 T, indicative of a mineral with relatively high coercivity, such as hematite, pyrrhotite or goethite.

4.2. Magnetic Remanence Directions

[25] Drill cores were cut into standard specimens of 2.5 cm in diameter and 2.2 cm in length. From a pilot set of 60 samples, thermal demagnetization proved better than alternating field (AF) demagnetization to clean the magnetic remanence. However, poorly consolidated samples, as well

as hand oriented samples housed within plastic boxes, were not amenable by thermal demagnetization and were processed using AF demagnetization. In all, 605 specimens were stepwise demagnetized using an average of 11 steps using either thermal (390 specimens) or AF (215 specimens) demagnetization. Magnetic remanences were either measured with a JR-5A automatic spinner magnetometer at the Laboratoire du Magnétisme des Roches d'Orléans (LMRO) or a 2G, three-axis DC SQUID magnetometer at the Institute de Physique du Globe de Paris (IPGP). Natural remanent magnetization (NRM) ranges from 0.113×10^{-3} A/m to 163×10^{-3} A/m, with an average of $7.8 \pm 8.9 \times 10^{-3}$ A/m. Magnetization components were determined by principal component analysis [*Kirschvink*, 1980] and the mean directions were computed using Fisher statistics [*Fisher*, 1953] with the paleomagnetic software packages of *Cogné* [2003] and R. Enkin (unpublished freeware).

[26] Figure 5 shows representative *Zijderveld* [1967] plots for samples treated with thermal and AF demagnetization. Both demagnetization techniques usually isolated a component at low temperature (<300°C) (Figures 5a to 5j) or low fields (<10 mT) (Figures 5k and 5l) that have variable, but mostly east or west (sometimes south in normal polarity samples) pointing declinations with fairly steeply downward dipping inclinations (Figures 5a and 5b). But contrary to what we observed at the neighboring Kuitun section, most samples (~90%) from Jingou have only minor or no low-temperature components. After the removal of this low component in the first few steps, thermal and AF demagnetization isolates a component between ~300°C to 690°C and >10 mT, respectively, that usually decays univectorally toward the origin on orthogonal diagrams (Figures 5a–5f, 5k, and 5l).

[27] The high unblocking temperature of 680°C is characteristic of hematite. However, on average, 75% of the natural remanent magnetization (NRM) intensity was removed by 590°C, which suggests that magnetite also contributes to the total remanence of the rocks. Because magnetization directions above and below 580°C are similar in the samples, both magnetite and hematite recorded the same magnetic field direction.

[28] Among the 605 demagnetized samples, 453 have linear magnetic components that decay to the origin (see auxiliary material[1] Data Set S1). Of the 453, 205 samples have normal polarities, 204 have reverse polarities and 44 have directions lying >60° from the overall mean direction that are interpreted as having recorded a transitional geomagnetic field (Figure 5j). Of the samples not possessing a magnetization component that trends toward the origin, 119 have remanent direction trajectories that follow great circle paths (Figures 5g and 5h) and 33 have unstable magnetizations with weak NRM intensities (Figure 5i). Of the 453 samples with linear components, samples interpreted as having recorded a transitional geomagnetic field (Figure 5j) were excluded when calculating the overall mean direction. Hand oriented samples collected from the upper part of the section were also omitted because of larger degrees of uncertainty associated with their orientations. In geographic coordinates, Fisher statistics on the 273 remaining samples yields declination $D_g = 353.8°$, inclination $I_g = -0.2°$, the best estimate of the precision parameter kg = 15.9, and the radius that the mean direction lies within 95% confidence $\alpha_{95g} = 2.2°$, while in stratigraphic coordinates, the values are $D_s = 348.5°$, $I_s = 53.1°$, $k_s = 15.1$ and $\alpha_{95s} = 2.3°$ (Figures 6a and 6b). The mean of the normal polarity ($D_N = 347.3°$, $I_N = 59.5°$ $\alpha_{95N} = 2.6°$) population is different at 95% confidence limits from both the present Earth's field and geocentric axial dipole field directions.

[29] The reversal test on the 273 samples is negative at the 95% confidence level [*McFadden and McElhinny*, 1990] because of a 14° difference in inclination between the normal and reverse polarities ($D_N = 347.3°$, $I_N = 59.5°$ $\alpha_{95N} = 2.6°$; $D_R = 169.3°$, $I_R = -46.9°$, $\alpha_{95R} = 3.4°$). This is likely produced by partially unremoved recent field magnetization that, because of the bedding geometry, may steepen the normal polarity directions and shallow the reverse ones. With that said, the lack of a significant LTC makes this interpretation slightly puzzling.

[30] Of the five sites collected from the northern flank of the Anjihai He anticline, only samples from three possessed stable magnetizations (sites A, B, and C in Table 1). These yielded similar demagnetization characteristics as those from the magnetostratigraphic section. In order to perform a meaningful fold test, we divided the lower part of the Jingou River section (where we collected samples by drilling) into 8 sites, with each site representing ~250 m in thickness (see Table 1). Figures 6c and 6d show the 11 site-mean directions before and after bedding corrections, respectively. The precision parameter increases 12 times after bedding correction ($D = 349.4°$, $I = 50.9°$, $k = 36.6$, $\alpha_{95} = 7.3°$) than before ($D = 351.1°$, $I = 17.8°$, $k = 3.0$, $\alpha_{95} = 30.6°$). The fold test is positive at 99% confidence limits [*McFadden*, 1990]. Despite the negative reversals test, the positive fold test, together with the abundant number of reversals, likely indicate the magnetic remanence is primary.

4.3. Magnetostratigraphy

[31] We established the magnetic polarity sequence of the Jingou River section using the 453 samples interpreted as having primary magnetizations whose components were defined by best fit line segments (Figures 7a and 7b), including those interpreted as having transitional directions. In the upper part, where samples were collected by hand, we also included 26 samples which yielded great circle trajectories but whose trends clearly identified the polarity. Magnetic chrons were based on a minimum of two successive horizons possessing the same polarity. Samples were not assigned a polarity if they possessed transitional directions (i.e., directions that fall outside our 60° criteria). When polarity changes are constituted by just a single horizon, we demagnetized the second sample from this horizon to confirm the polarity. Polarity events documented by only one horizon were represented in gray in Figure 7 and given less weight when correlating the Jingou River magnetic polarity

[1] Auxiliary materials are available in the HTML. doi:10.1029/2007TC002137.

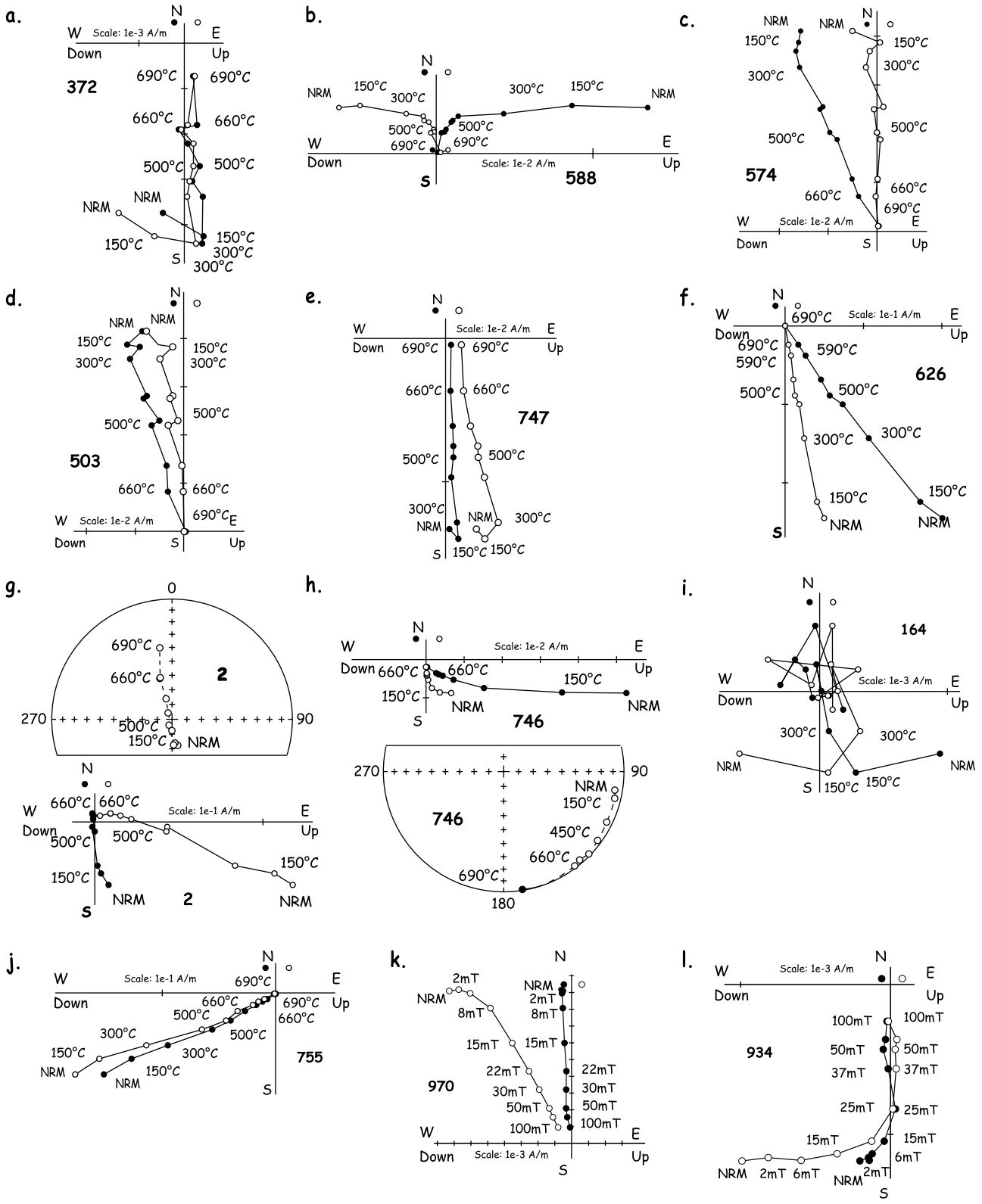

Figure 5. Representative Zijderveld diagrams [*Zijderveld*, 1967] obtained from both thermal and alternating field (AF) demagnetization (in situ coordinates).

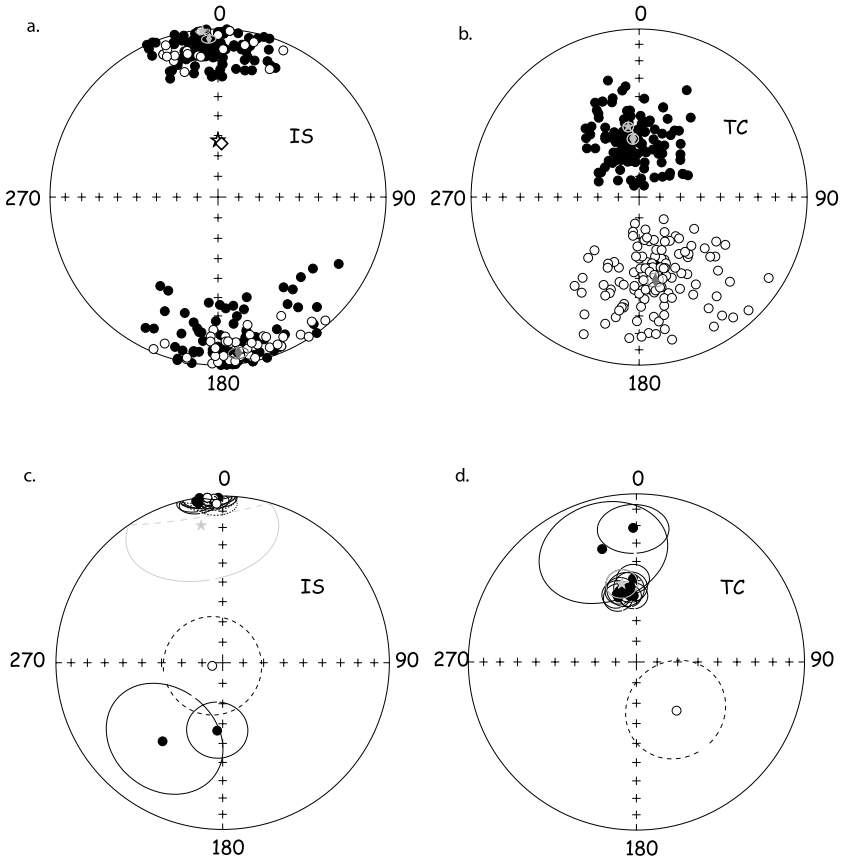

Figure 6. Equal-area projections of the principal component directions (a, b) of the 273 samples collected with a gasoline power drill and having stable component not considered as transitional and (c, d) of the 11 mean directions used to perform the fold test, in in situ and tilt corrected coordinates, respectively. Diamond in Figure 6a shows the mean direction for each polarity while the gray (open) stars represent the (overall) mean directions in both polarities. White diamond and star in Figure 6a represent the present-day Earth's magnetic field (PDF) and the geomagnetic axial dipole (GAD) directions, respectively.

Table 1. Site-Mean Paleomagnetic Directions From This Study[a]

Site	Thickness (m)	n	D_g (deg)	I_g (deg)	D_s (deg)	I_s (deg)	k	α_{95} (deg)
Mean	2075–4572	273	353.8	−0.2	348.5	53.1	15.1	2.3
1	2330–2580	42	350.7	2.1	343.8	55.5	13.5	6.9
2	2580–2830	42	356.9	3.1	354.4	57.6	18.4	5.3
3	2830–3080	30	358.5	1.1	357.7	57.6	17.4	6.5
4	3080–3330	28	357.0	−1.6	355.5	53.1	13.6	7.7
5	3330–3580	33	352.0	0.2	346.7	54.1	14.9	6.7
6	3580–3830	27	351.4	3.5	344.3	57.2	17.4	6.9
7	3830–4080	24	354.7	−0.7	351.5	54.0	12.9	8.6
8	4080–4572	47	357.8	−5.1	357.7	48.9	15.0	7.4
A	-	6	184.6	56.4	358.6	21.3	22.8	14.3
B	-	4	217.4	40.4	343.1	30.5	12.0	27.7
C	-	7	253.3	−84.7	140.5	−59.2	7.2	24.1
Average	-	-	351.1	17.8	-	-	3.0	30.6
Average	-	-	-	-	349.9	50.9	36.6	7.3

[a]Sites A–C come from the northern flank of the Huo'erguosi anticline. Subsections 1 to 8 come from the magnetostratigraphic section, with each subsection representing roughly 250 m in thickness. Abbreviations are n, number of samples; D, magnetic declination; I, magnetic inclination; g, geographic coordinates; s, stratigraphic coordinates; k, precision parameter; α_{95}, radius of the cone in which the mean direction lies within 95% confidence.

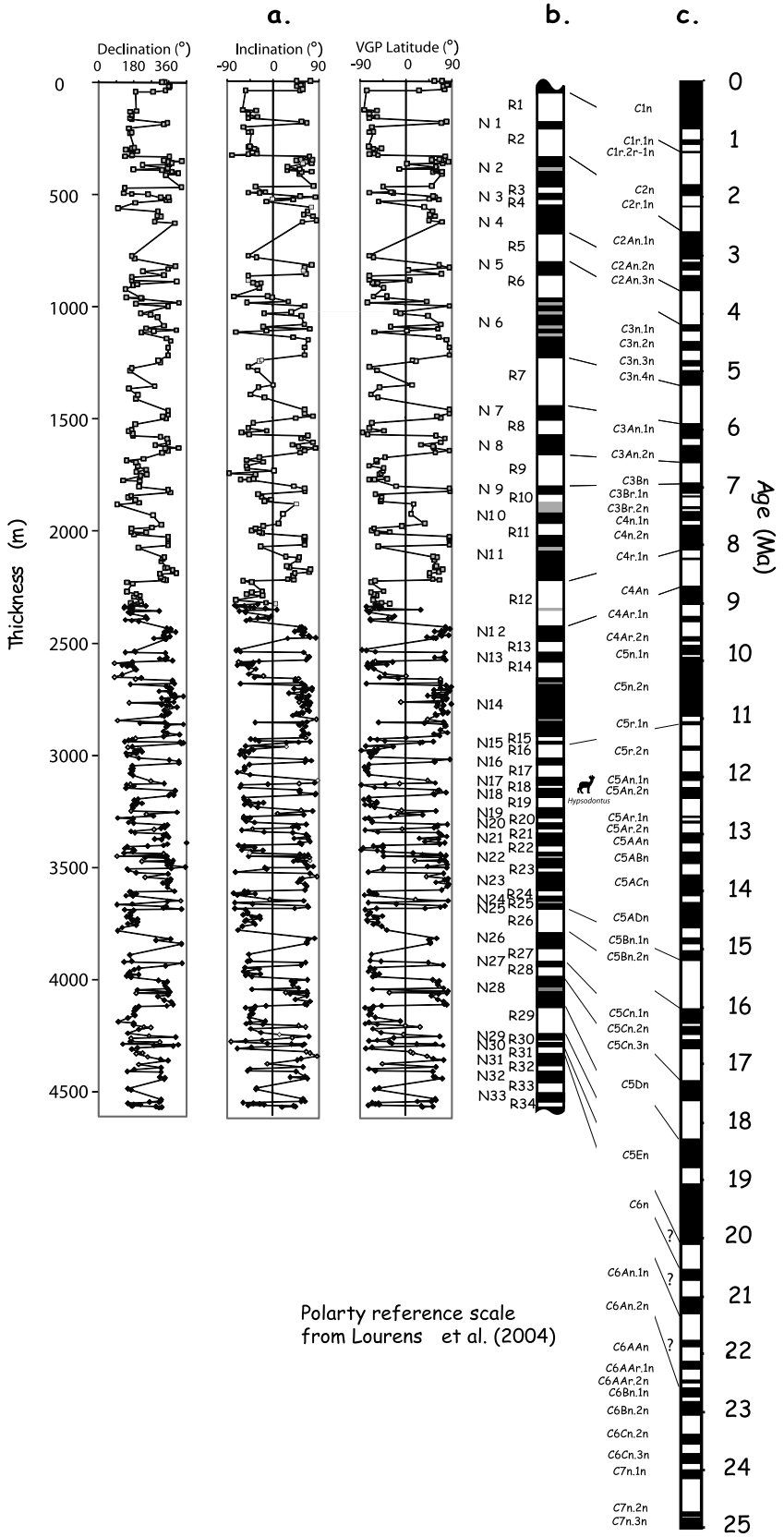

Figure 7. (a) Paleomagnetic directions (declination and inclination) obtained using principal component analysis. (b) Magnetostratigraphic column from this study. (c) Reference polarity timescale [after *Lourens et al.*, 2004].

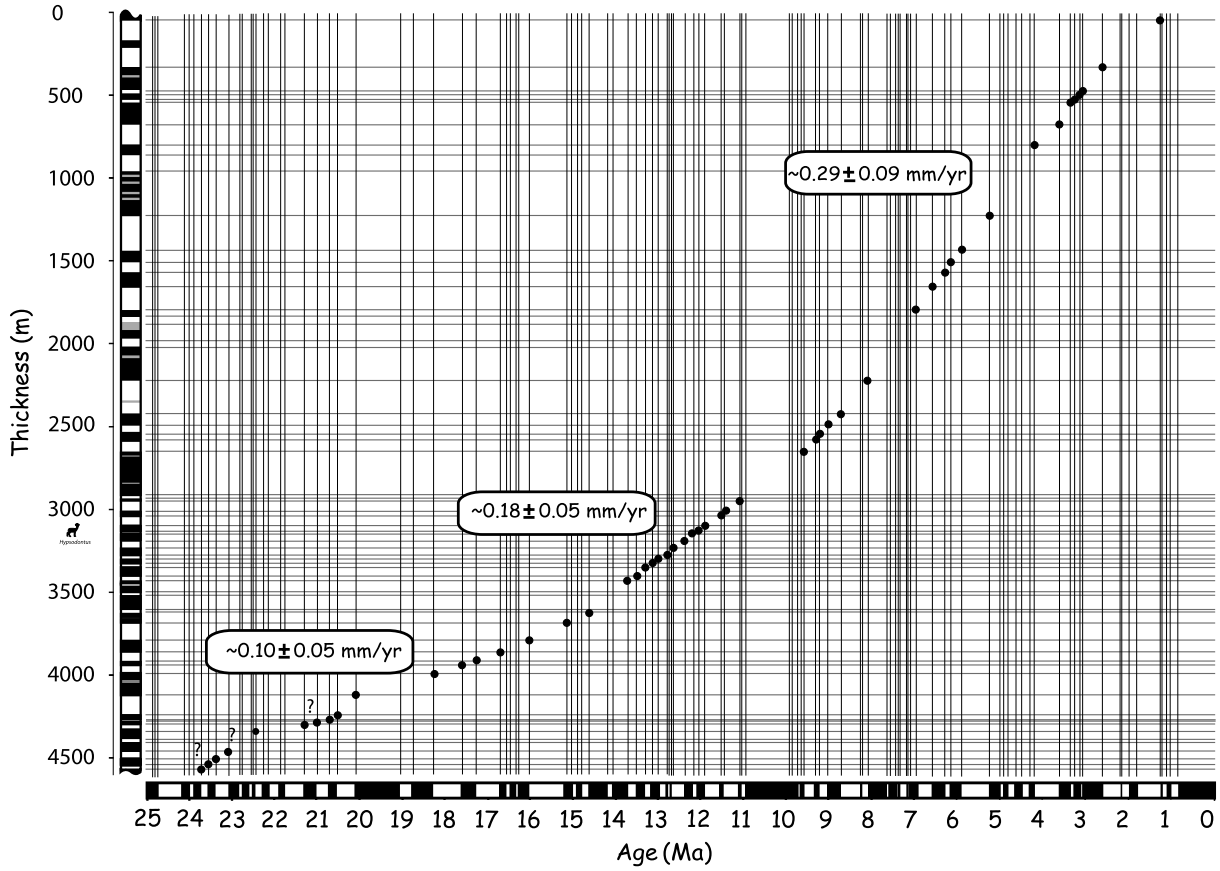

Figure 8. Age versus depth plot of the Jingou River section, using the data and correlation from Figures 7b and 7c.

column with the reference geomagnetic polarity timescale. Thus, 33 normal magnetic chrons (N1 to N33) and 34 reverse ones (R1 to R34) were identified (Figure 7c). We correlated the Jingou River magnetostratigraphic sequence to the *Lourens et al.* [2004] reference polarity timescale following three criteria: (1) the high number of reversals likely places the section in the middle to upper Tertiary; (2) the presence of six chrons of duration: two reversed (R7 and R12) and four normal (N2, N4, N14 and N28) (Figure 7b); and (3) the discovery of *Hypsodonthus sp.* at 3165 m depth (see stratigraphic location on Figure 7b) likely indicates a middle Miocene age.

[32] Figures 7c and 8 present our preferred correlation. A relatively good match occurs between chrons C4n.1n and C6A.1n except for one or two missing reversed polarity chrons within normal chrons N14, N19, N26, and N28. Except for N28, these missing intervals are likely because of their relatively short durations, lasting from 100 to 40 ka. Indeed, the recording of rapid geomagnetic excursions or short polarity events depends on sedimentation rate [*Roberts and Winklhofer*, 2004]. However, the missing reversed polarity chron N28, that lies between reference chrons C5En and C6n, is longer, and would represent a hiatus of ~22.4 m (given an average sedimentation rate of ~0.1 mm/a in this part of the section). Moreover, no important sampling gap in this part of the section can explain why it is missing.

[33] On the other hand, reverse polarity chrons were identified within the normal polarity chrons N14 and N28 but were defined only by a single sample (gray zones in the magnetostratigraphy column of Figure 7b) so they were not included in our scale. Moreover, one sample within normal polarity chron N19 has a very low positive inclination (9.5°) and southward declination (240°) that could correspond to a transitional field surrounding a reversed event that was missed. Given the average sediment accumulation rates (see below), the two missing reversals events within chron N26 would represent ~7.1 m and ~3.5 m in equivalent time. They could have been easily missed because of sampling gaps of ~30 m in this part of the section.

[34] The correlation of the bottommost part (<4200 m) of our section remains tentative leading to some discrepancy in sedimentation rate (see Figure 8). Several events are missing (C6A.An and C6Aar.1n) below the reference chron C6An.1n. This is again likely explained by the lower number of horizons that possess stable magnetic remanences in this part of the section (<~0.2 sample/m), sampling gaps of ~20 m on average because of sample collection problems and lower sediment accumulation rates (0.1 mm/a). However, our sedimentological analyses suggest continuous sedimentation with no evidence for any significant hiatus. In the uppermost part (<2400 m), where samples were taken by hand, the correlation remains relatively good despite

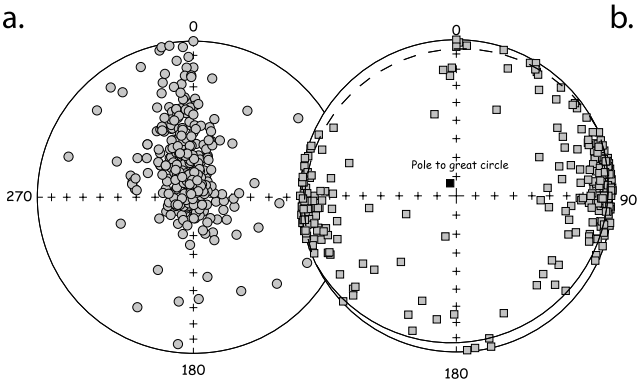

Figure 9. Stereonet projections of the anisotropy of magnetic susceptibility principal axes: (a) maximum (k1) (circle) and (b) minimum (k3) directions (square) (all in tilt-corrected coordinates).

some missed events (again probably because of the relatively low sampling density).

[35] To conclude, our correlation delimits the Jingou River magnetostratigraphy section between chrons C1r.1n and C6n.3n on the *Lourens et al.* [2004] reference scale. This correlation dates the sampled sediments in an absolute reference frame from ~1 to ~23.6 Ma. Figure 8 shows the deposition rate of the Jingou River section. A net increase through time is quickly apparent, giving average sediment accumulation rates of 0.1 ± 0.05, 0.18 ± 0.05 and 0.29 ± 0.10 mm/a from >23.6 to ~16–15 Ma, from ~16–15 to ~11–10 Ma and from ~11–10 Ma to <1 Ma, respectively (Figure 8). An important question is whether the increasing trend occurs continuously or in steps. To resolve this, we plotted the instantaneous sediment accumulation rates in Figure 10a. It appears that the data tend to cluster in distinct regimes about a mean value rather than defining a linear or exponential increase, especially concerning the change at ~16–15 Ma. An abrupt acceleration near the upper part of the section is more loosely constrained at ~11–10 Ma because of the long duration of the C5n.2n normal chron.

4.4. Anisotropy of Magnetic Susceptibility

[36] The anisotropy of magnetic susceptibility (AMS) of 323 samples was measured with an AGICO KLY-3S Kappa-Bridge. The hand samples were not measured because the plastic boxes obscure the signal. Bulk magnetic susceptibility (κ) ranges from 76 to 1682 $\times$ 10^{-6} SI with an average of 548 ± 297 $\times$ 10^{-6} SI. Figure 9 shows stereonet projections of the principle maximum (k1) and minimum (k3) principal axis. The k1 and k3 directions are well grouped. The k1 axes generally strike east–west with a low inclination (<30°) and parallel the strike of the fold axis. The k3 axes remain subvertical with a slight tilting (~14°) to the north. This pattern is commonly found in folded sediments in particular into foreland basin and attest to a weak tectonic overprint of the original sedimentary fabrics [*Kanamatsu et al.*, 1996; *Kodama*, 1997; *Parès and Van der Pluijm*, 2002; *Robion et al.*, 2007].

[37] From the AMS analyses one can easily calculate different magnetic parameters such as bulk magnetic susceptibility (κ), the degree of anisotropy (P_j) [*Jelinek*, 1981], and the mean shape of the anisotropy ellipsoid, called the T parameter [*Hrouda*, 1982]. Interestingly, variations in κ roughly follow changes in sedimentation rate where three different regimes occur (Figure 10b). One lies from 22 Ma to ~15 Ma where κ progressively decreases before stabilizing around 300 $\times$ 10^{-6} SI. At ~15 Ma, κ rapidly increases to ~500 $\times$ 10^{-6} SI and remains stable until ~11 Ma where κ jumps in magnitude to ~800 $\times$ 10^{-6} SI then stays fairly constant until the top of the section. We recall that the magnetic mineralogy experiments found that both magnetite and hematite contribute to the magnetic remanence in the Jingou River sediments. The magnetic susceptibility of magnetite is ~1000 times greater than most other minerals, so the evolution of κ probably depends mostly on magnetite concentration. This would imply that changes in source rock occurred punctually albeit with a trend toward increasing amounts of magnetite.

[38] From the AMS measurements, the degree of anisotropy (P_j) [*Jelinek*, 1981] is believed to be sensitive to lithology (such as clay content) or strain (from compaction, etc.), whereas the shape parameter (T) [*Hrouda*, 1982], which describes the shape of the AMS ellipsoid, is related to the preferred orientation of multiple grains [e.g., *Martin-Hernandez et al.*, 2004]. Thus, T can provide information related to the hydrologic regime and transport conditions experienced by the sediments [e.g., *Kissel et al.*, 1997; *Gilder et al.*, 2001; *Charreau et al.*, 2005, 2006]. At the Jingou River section, P_j ranges from 1.004 (4%) to 1.078 (8%) with an average of 2 ± 1%. P_j remains relatively constant from the base to top of the section (Figure 10c). However, the scatter of P_j is greater from 22 to 21 Ma to ~15–14 Ma and after 11–10 Ma, whereas P_j varies less from ~15–14 Ma to ~11–10 Ma. T undergoes distinct changes at the Jingou River (Figure 10d). T is close to zero at the base of the section to ca. 20 Ma then trends progressively toward distinctly positive (oblate) values until ca. 15 Ma when it slowly goes back to 0. At ~14 Ma, T again progressively rises to positive values, reaching 0.4 by 12 Ma then remaining at around 0.4 until the top of the section. In order to track possible changes in the principle axis directions related to the changes in the AMS parameters, we divided the section into four different parts where the T parameter changes. We then calculated the overall mean directions of the k1 and k3 axes for each part (Figure 11). Despite changes in the AMS parameters, the AMS principle axis directions remain relatively constant (Figure 11), and thus independent of the shape or magnitude of the anisotropy ellipse.

5. Sedimentological Analysis and Age Constraints on the Neogene Stratigraphy of the Southern Junggar Basin

[39] On the basis of a preliminary analysis of lithology and sedimentary structures, 12 faciological units were identified in the Jingou River magnetostratigraphic section (Figure 12). These units are briefly described below, from the bottom to the top of the section, and interpreted in term of depositional processes and environments.

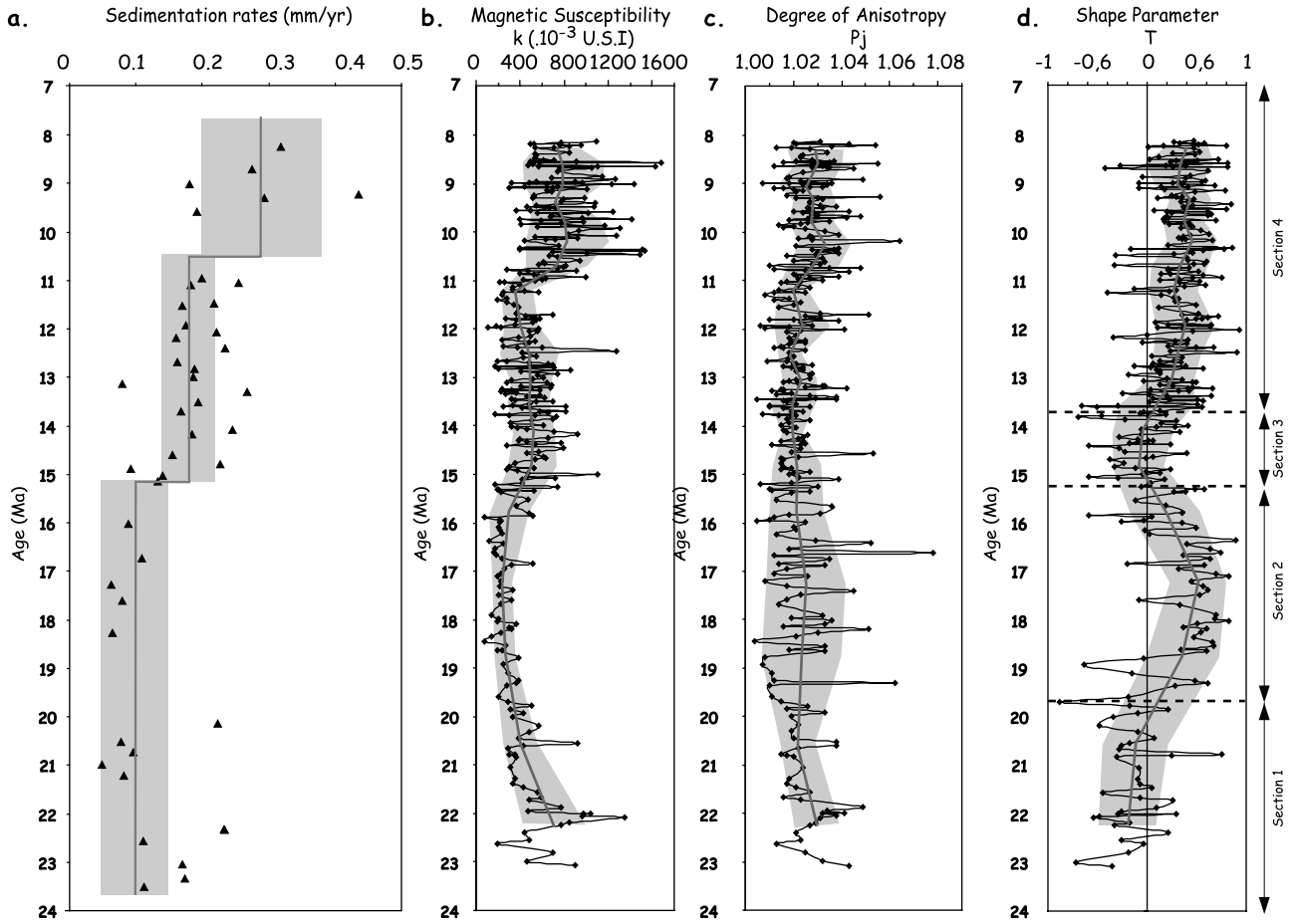

Figure 10. (a) Variations in sedimentation rate, (b) the magnetic susceptibility (κ), (c) the degree of anisotropy (P_j), and (d) the shape parameter (T), as a function of time for the Jingou River section. Heavy solid line shows the average of a sliding window shifted every 50 m; 1σ uncertainties in gray.

[40] Cenozoic sediments from south Junggar are mainly continental in origin, and thus notoriously lacking in fossils; most age constraints of these sediments are based on grain size and sediment color correlation from a few sections where fossils (mainly mammals and ostracods) have been found [e.g., *BGMRX*, 1993]. Thus, our sedimentological analysis is useful to better constrain the limit of the different stratigraphic formations in terms of environmental changes. Moreover, our magnetostratigraphic study provides indispensable information to place the Neogene stratigraphy of southern Junggar in an absolute time frame.

[41] At the base of the Anjihai formations, unit 1 corresponds to a stack of green silty marls (decimeters to a few meters thick), mudstones (centimeters to a few decimeters) and bioclastic beds (centimeters to a few decimeters), rich in freshwater gastropods. This first facies attests to a freshwater, carbonate-rich biogenic production deposited in a reducing environment. This implies the existence of a carbonaceous reducing lacustrine system at the beginning of the sedimentary history of the studied section. This unit gradually shifts into unit 2 of a series of green silty marls (decimeters to a few meters thick), mudstones (centimeters to a few decimeters) and bioclastic beds (centimeters to a few decimeters) rich in freshwater gastropods but mixed with vertebrate (e.g., turtle) bones and medium to coarse-grained sand. In its upper part, unit 2 exhibits massive to graded or laminated, medium to coarse sandstones (a few centimeters to decimeters), generally overlain by homolithic, ripple to cross-bedded, coarse sandstones (a few decimeters to meters) over slightly erosional surfaces. This second facies association is also reminiscent of a carbonaceous reducing lake but with terrigenous supplies provided by subaqueous currents. A sharp transition occurs between units 2 and 3 marked by a total change in lithology and color, from green silty marls to red clay-rich fine-grained siltstones. This marked color change is used in this paper and previous Chinese publications [e.g., *BGMRX*, 1993] as the limit between the Anjihai and Shawan formations. Our magnetostratigraphic section commenced near the bottom of the Shawan formation, placing it roughly between the Oligocene to Miocene epochs at ~23.6 Ma.

[42] At the base of the Shawan Formation, unit 3 comprises a series of red clay-rich siltstones (decimeters to meters thick), massive to laminated or rippled, medium to coarse sandstones (a few centimeters) and homolithic, rippled to cross-bedded, coarse sandstones to granular conglomerates (a few decimeters to meters) deposited over slightly erosional

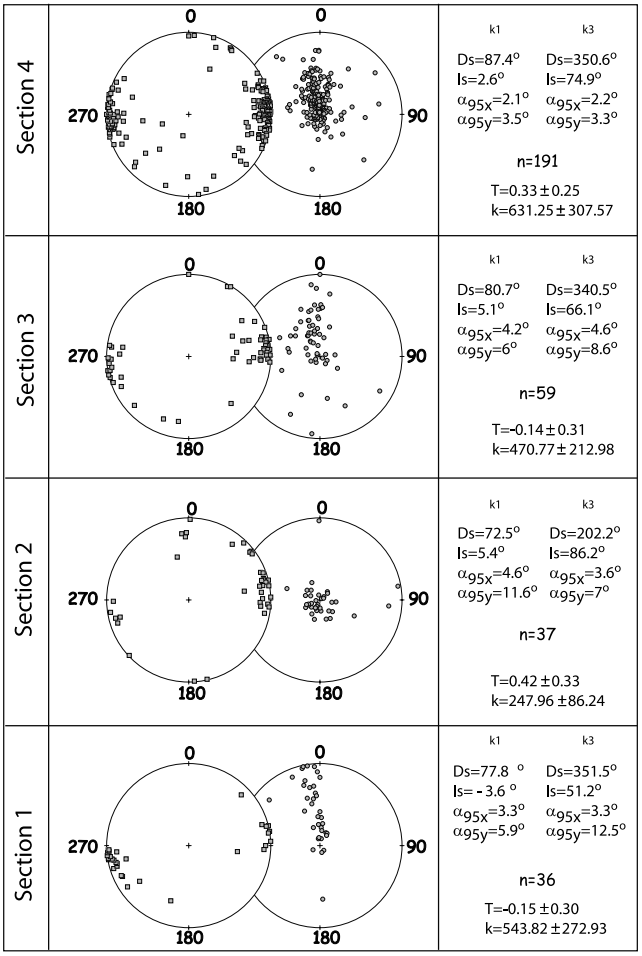

Figure 11. (left) Equal-area stereonet projections of the anisotropy of magnetic susceptibility principal maximum k1 (square), and minimum k3 directions (circle) for the four sections defined in Figure 9, which are defined by variations in their AMS parameters. (right) The mean direction of both k1 and k3 using bivariate statistics [*LeGoff et al.*, 1992] and means with 1σ uncertainties of AMS magnetic parameters T and κ.

surfaces. On the basis of our preliminary analysis, these facies may be linked to a subaqueous, terrigenous setting with subaqueous to subaerial currents and are tentatively interpreted as being deposited in a terrigenous oxidizing lacustrine environment near a fluvial system. At its top, unit 3 shifts quickly (few meters) to unit 4, which is composed of a series of laminated algal limestones (a few centimeters to decimeters thick), red clay-rich siltstones (a few centimeters to a few decimeters) and massive to rippled, medium to coarse-grained sandstones (a few centimeters to decimeters) disrupted by homolithic, massive to horizontal and cross-bedded, coarse sandstones to pebble conglomerates (a few decimeters to a few meters) that lie over erosional surfaces. The siltstones and medium to coarse sandstone layers are often extensively bioturbated and exhibit numerous burrows and potential root tracks. This fourth facies association shows the occurrence of subaerial channel and overbank flows in a place where water can stand and where life (bacterial, animal and vegetal) developed. The sedimentary environment was likely a fluvial floodplain system with swamps rich in life. Upward, unit 4 shifts to unit 5 over a short transition (a few meters). Unit 5 includes red massive siltstones (a few centimeters to a few decimeters thick) and massive to rippled, medium to coarse-grained sandstones (a few centimeters to a few decimeters thick), intercalated with homolithic, massive to horizontal and cross-bedded, coarse sandstones to pebble conglomerates (a few decimeters to a few meters thick) all being deposited over erosional surfaces. Those deposits are because of channel and overbank flows in a subaerial environment corresponding to a fluvial system with a floodplain. Unit 5 grades quickly (few meters) into unit 6; the transition is marked by the reappearance of green layers of silty marls. We fix the first occurrence of those marls as the limit between the Shawan and Taxihe formations, dated here at $\sim$20.1 Ma.

[43] At the base of the Taxihe Formation, unit 6 exhibits alternating facies associations found in units 2 and 3. This alternation points to cyclic changes of sedimentary environments from a terrigenous oxidizing fluvial to lacustrine system, to a carbonaceous reducing one, but still with episodic terrigenous supplies. In the lower part of unit 6, unit 2-like facies are scarce and form only thin layers (a few decimeters thick). Toward the top, these layers get thicker (meters to a few meters) and unit 3-like facies quickly disappear to give way to unit 7, where only the unit 2-like facies crop out. This seventh unit corresponds therefore to the establishment of a carbonaceous reducing lacustrine system with terrigenous supplies provided by subaqueous currents. On top of unit 7, unit 3-like facies reappear, and an alternation of the unit 2 and 3 (and minor unit 11) facies associations is again exposed, extending into unit 8. As for unit 6, this indicates alternations of depositional environments from a carbonaceous reducing lake with terrigenous supplies to a terrigenous one close to a fluvial system. Unit 8 turns into unit 9 over a short distance (a few meters) emphasized by the disappearance of the green silty marls. In this paper, the last occurrence of those marls is considered to be the limit between the Taxihe and Dushanzi formations, that we dated at $\sim$16 Ma.

[44] At the base of the Dushanzi Formation, unit 9 consists of unit 3-like (and minor unit 10-like) facies and our preliminary interpretation for the sedimentary environment of these deposits is also a terrigenous oxidizing lake near a fluvial system. Unit 9 shifts quickly (a few meters) to unit 10, which is composed of red siltstones (a few centimeters to a few decimeters thick) and massive to rippled, medium to coarse sandstones (a few centimeters to decimeters thick), intercalated with homolithic, massive to horizontal and cross-bedded, coarse sandstones to pebble conglomerates (a few decimeters to a few meters thick) over erosional surfaces. Into this unit, the siltstones and medium to coarse sandstone layers are again extensively bioturbated and exhibit numerous burrows and potential root tracks. This facies association thus shows the occurrence of subaerial channel and overbank flows in a setting where abundant life developed. Upward, this tenth unit gradually shifts to a new one. Unit 11 includes

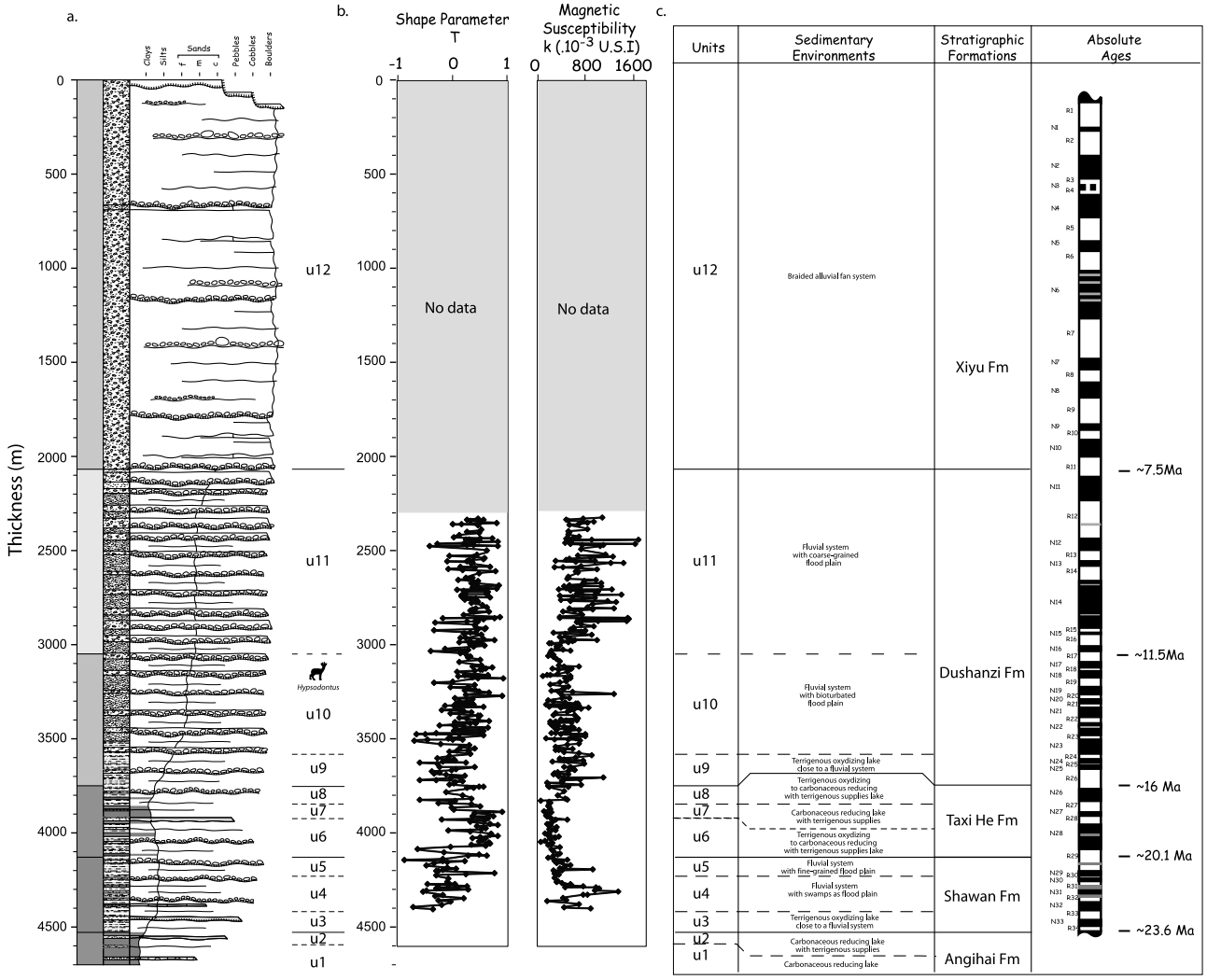

Figure 12. (a) Synthetic sedimentological column of the Jingou River section. (b) Depth evolution of shape parameter T and magnetic susceptibility κ. (c) Comparison of the lithological units, stratigraphic formations and magnetostratigraphic ages.

orange, massive, fine sandstones (a few centimeters to a few decimeters thick) and massive to rippled, medium to coarse sandstones (a few centimeters to a few decimeters thick), disrupted by homolithic, massive to horizontal and cross-bedded, granule to cobble conglomerates (few decimeters to a few meters) over strongly erosional surfaces. Those coarse deposits are because of powerful channel and overbank flows in a subaerial environment corresponding to a fluvial system with a coarse-grained floodplain.

[45] At the Jingou He section, the Xiyu Formation (unit 12) consists of rare, orange, massive to horizontal and cross-bedded, medium to coarse sandstones (decimeters to a few meters thick), in between homolithic, massive to horizontal and cross-bedded, granule to block conglomerates (a few decimeters to a few tens of meters) deposited over strongly erosional surfaces, cutting at maximum 1–2 m into the underlying sediments. This very coarse facies association attests to the occurrence of powerful braided streams in a subaerial environment corresponding to a fan-shaped braided fluvial system.

[46] Unit 11 gradually gives way to unit 12 over a span of ~250 m. The sedimentary environment progressively evolved from fluviatile system with powerful braided streams and overbank flows to a fan-shaped braided fluvial system dominated by powerful braided streams. We found no evidence for a hiatus within this progressive sedimentary environmental transition between the Dushanzi and Xiyu formations. The limit between those two units is considered to be the point where the conglomeratic exceeds ~75%, which is also our criteria to fix the limit between the Dushanzi and Xiyu formations.

[47] A few more sedimentary units at the top of the Jingou River section probably correspond to late Quaternary and river terraces [*BGMRX*, 1993]. Those deposits show the same facies association as unit 12 but are sometimes interbedded with yellow, massive to horizontal and cross-bedded,

loess (decimeters, few meters thick), rich in pebbles and cobbles. The association of this facies with that of unit 12 points to a mixing of sediments transported by wind and powerful subaerial braided streams. The corresponding sedimentary environment is a braided fluvial fan system with aeolian deposition between active channels.

6. Discussion

6.1. Implications for the Cenozoic Uplift History of the Central Tian Shan

6.1.1. Early Stage of Deformation During the Early Miocene

[48] The sedimentological analyses show that the first appearance of a significant detrital input into the foreland basin may occur at ~24 Ma (this ages needs to be handled with caution as our correlation at the bottom of our section from ~23.6 Ma to ~20 Ma remains tentative below the bottom of unit 2). This could indicate that the Tian Shan underwent both rapid uplift and erosion at that time. However, sedimentological analyses at a single section should be viewed cautiously, as sedimentary environments in continental basins may present large variability along strike of the range.

[49] Sedimentary accumulation reconstructions [*Métivier et al.*, 1999], paleocurrent analysis [*Hendrix et al.*, 1992] and isopach maps [*BGMRX*, 1993] suggest that the Junggar basin was mainly filled by sediment shed from the Tian Shan range. Rapid discharge of sediments stored in intramountain basins within the Tian Shan (e.g., Bayanbulak, Figure 1) through river network reorganization, could contribute to heightened flux within the foreland basin, but the volume of these basins is negligible compared to the size of the Tarim and Junggar basins. So, a prolonged acceleration in sediment flux is normally coupled with an acceleration in erosion. Because good chronological constraints from continental sediments are rare, detailed knowledge of the evolution of the sedimentary flux remains vague. To progress further in deciphering the Tian Shan history from the sedimentary record, one must assume that changes in sedimentary flux should generate changes in sedimentation rate and that variations in sedimentation rate are recorded by variations in sediment accumulation rates. *Métivier et al.* [1999] pointed out that 1-D sediment accumulation rates derived from a drill hole (or cross section) should be handled with caution since the sedimentation rate at one point may not correlate with the total sediment flux delivered to the basin, especially in the case of continental basins. Indeed, hydrologic network reorganization or modification of local accommodation space driven by fault activation (through thrust fault propagation) or basin subsidence may also generate changes in sedimentation rate along a single profile.

[50] First let us assume that sedimentation rate is a proxy for sediment flux eroded from the range keeping in mind that independent data are needed. In this case, changes in sedimentation rate may be interpreted as accelerations in erosion and/or uplift rates of the Tian Shan range. Unfortunately, our magnetostratigraphic analyses do not provide information prior to 24 Ma and remains tentative until ~21–20 Ma. From ~20 Ma to 15 Ma the sedimentation rate was constant but relatively low (<0.1 mm/a) when compared with other rates (0.2–0.5 mm/a) found at the front of active mountain ranges [*Opdyke et al.*, 1979; *Appel et al.*, 1991; *Gilder et al.*, 2001; *Charreau et al.*, 2005, 2006]. This seems to contradict the sedimentary analysis which shows an increase in detrital input at the bottom of unit 2, around ~24 Ma. But this absence of increase in sedimentation rate may be explained by the fact that, before unit 2, lower detrital input may have been compensated by a biogenetic and chemically driven in situ production which yielded higher sedimentation rates. Progressing upward in unit 2, the sedimentation becomes more clastic driven and strictly dependent on external input. More data are needed to clarify this ambiguity.

[51] AMS data can provide useful complementary information on variations of magnetic grains and sedimentary fabrics and thus may help to solve this dilemma. However, the magnetic fabrics of sediments may be modified by subsequent compaction or tectonism, thus obliterating the original sedimentary fabric. So, one needs to first ensure that no significant overprint occurred. If compaction or tectonism affected the rocks, one would expect that the strain would reorganize the magnetic fabric differently depending on the clay content or grain size of the sediments [*Kanamatsu et al.*, 1996; *Kodama*, 1997; *Gilder et al.*, 2001; *Parès and Van der Pluijm*, 2002]. As shown in Figure 9b, the degree of anisotropy (P_j) remains constant and is thus independent of lithology. Moreover, if the magnetic fabrics were influenced by compaction, one would expect that T should become more oblate as a function of depth and/or that P_j will increase as a function of depth. Neither is observed (Figures 10d and 10c).

[52] The AMS shape parameter T can provide information related to the hydrologic regime and transport conditions experienced by sediments [*Kissel et al.*, 1997; *Gilder et al.*, 2001; *Charreau et al.*, 2005, 2006]. Indeed, T can be sensitive to a preferred orientation of the particles acquired during deposition [e.g., *Martin-Hernandez et al.*, 2004]. When T is near 0, the particles were deposited in an environment where they acquired no systematic preferred orientation. Interestingly, the AMS principle axes directions and their uncertainties show no particular correlation with T (Figure 11), possibly suggesting that T is sensitive to the sum of the shape anisotropies of the individual grains. Changes in T going from spherical to oblate may imply hydrologic modifications in the catchment basin with higher stream capacity and/or closer sediment source, which will in turn bear on the shape anisotropy of the individual particles. This may be driven by tectonic or climatic changes in the range. Thus modifications of T could be associated with changes in the sediment flux delivered to the basins. For example, at the Yaha section [*Charreau et al.*, 2006] in the southern Tian Shan, the change in T occurred at ~11 Ma and was correlated with a major acceleration of the sediment accumulation rates at the same time.

[53] Following the hypothesis made above and on the basis of previous studies [*Charreau et al.*, 2005, 2006], the change of T at ~21–20 Ma could mean that hydrodynamic

reorganization occurred then. Sedimentological analysis within the Shawan Formation led to similar conclusions, as the sedimentary environment changes from a fluviatile system with swampy floodplain that probably favor decantation (unit 4) to a more dynamic fluviatile system with more active floodplains (unit 5). At ~17 Ma, *T* decreases to 0 by ~15 Ma, signifying a return to relative hydrodynamic quiescence. Indeed, from sedimentological analyses we find that, within the Taxi He Formation, the sedimentary environment progressively returns to a pure lacustrine (unit 7) from a fluviatile (unit 6) environment at ~17 Ma. Another piece of valuable information comes from magnetic susceptibility (κ), which is, to a first order, correlated to the nature and concentration of magnetite grains in sediments and is derived mostly from basement material. Again the magnetic susceptibility curves show no important modification from ~23.6 (?) Ma to ~16–15 Ma which likely means that source rock did not change significantly over this period, and thus there should be no source-dependent bias reflecting on the shape of the grains.

[54] Thermochronological studies of *Hendrix et al.* [1994] and *Dumitru et al.* [2001] have shown that by ~24 Ma the northern Tian Shan experienced uplift in some places. Moreover, from a rock magnetic and magnetostratigraphic study of two sections in the Kuche basin (South Tian Shan), *Huang et al.* [2006] identified important changes in rock magnetic parameters at ~20 Ma (without significant increase in sedimentation rates) which they related to beginning of faulting in the southern range. Several workers believe that by 25–20 Ma Asia underwent global tectonism reorganization with marked activation of several important faults [e.g., *Catlos et al.*, 2002; *Lacassin et al.*, 2004; *Tapponnier et al.*, 1990]. Despite limited constraints on sediment ages before ~20 Ma, fission track data suggest that by 25–20 Ma, the Tian Shan was uplifted, although it was relatively subdued because of the absence of marked sedimentation flux into the basin. Magnetostratigraphic analyses of Oligocene to early Neogene sediments from Junggar and Tarim are needed to better constrain this point.

6.1.2. Middle Miocene Uplift

[55] Our magnetostratigraphic analyses suggest that sedimentation rate doubled at ~16–15 Ma and again accelerated at ~11–10 Ma. Increases in sedimentation rate apparently happened more or less punctually rather than progressively (Figures 8 and 10a), remaining relatively constant between times of acceleration. The jumps in sedimentation rate may indicate heightened sedimentary flux because of uplift pulses that were accompanied by higher erosion rates. But again, because these are 1-D sedimentation rates, independent data are required to better understand the cause of the changes in sedimentation rate.

[56] At the Jingou River section, correlations between sediment accumulation rates and various magnetic parameters are rather satisfactory though with some discrepancies. The greatest acceleration in sedimentation rate at ~16–15 Ma is strongly correlated with a change in *T*. Then, from 15 Ma to top of the section, *T* remains greater than 0 as the high sediment accumulation rates persist. Moreover, at ~16–15 Ma, magnetic susceptibility (κ) strongly increases. So, by ~16–15 Ma coupled changes in *T*, κ and sedimentation rate suggest that the hydrodynamic regime became more energetic and was associated with modification in rock source and heightened sediment flux. Sedimentological observations agree well, as at ~16–15 Ma, the depositional environment progressively changed from lacustrine (unit 8) to fluviatile (units 9, 10, and 11). This coincides with the passage into the Dushanzi Formation with an initial transitional period (unit 9) and then, a clear fluviatile system with a coarse-grained floodplain that persisted across the Xiyu/Dushanzi limit (unit 12). We thus believe that the major deformation stage of the Tian Shan occurred at ~16–15 Ma as we observe both important hydrological and environmental changes and a long-term sedimentation rate acceleration at the Jingou River section. On the southern flank of the Tian Shan, *Huang et al.* [2006] also observed an acceleration in the sedimentation rate at ~15 Ma. In the Aksu area (west Tarim), magnetostratigraphy also points to rapid acceleration of the sediment accumulation rates at this time [*Heermance et al.*, 2007].

[57] We also find another acceleration in sedimentation rate at ~11–10 Ma that remains constant at 0.29 ± 0.10 mm/a until the top of the section (~1 Ma). So, sedimentation rate probably remained relatively stable until recent times, which is what we observed at the Kuitun section with constant rates from ~10.5 Ma until ~3.1 Ma [*Charreau et al.*, 2005]. However, the average sedimentation rate at the Kuitun section is lower (~0.21 mm/a) [*Charreau et al.*, 2005]. This may be explained by the fact that the Kuitun section lies at a greater distance from the front range than the Jingou River section.

[58] However, the change at ~11 Ma is not correlated with a significant modification either in the *T* parameter or in the sedimentary environment. By ~11 Ma, as shown by the evolution in κ, the magnetite content of the sediment rapidly increased and bioturbation ceased (unit 11), which indicate that some environmental or source change occurred at this time. Our magnetostratigraphic study in the Kuche basin (south Tian Shan) revealed an important increase in sedimentation rate at ~11 Ma associated with a change in *T* parameter from spherical to oblate [*Charreau et al.*, 2006]. Moreover, the Chu section in the Kyrgyz Tian Shan also exhibits a significant increase in sedimentation rate at ca. 11 Ma, associated with higher denudation rates of the range as deduced from U-Th/He thermochronology [*Bullen et al.*, 2001, 2003]. Recently, apatite fission track analyses on three transects from the eastern Kyrgyz Tian Shan demonstrated that the range propagated over 110 km eastward over the last ~7–11 Ma [*Sobel et al.*, 2006]. Thus the hypothesis that the Tian Shan underwent uplift and erosion acceleration that started by ~11–10 Ma seems robust.

6.2. Significance of The Xiyu Formation: Arguments Against a Plio-Pleistocene Uplift of the Tian Shan

[59] The Xiyu conglomerate is widely distributed in central Asia. It was dated as Plio-Pleistocene on the basis of a single finding, at the transition between the Dushanzi and the Xiyu formations, in the nearby Anjihaihe section (Figure 2) [*Chen et al.*, 1994], of *Equus sameniensis*, which

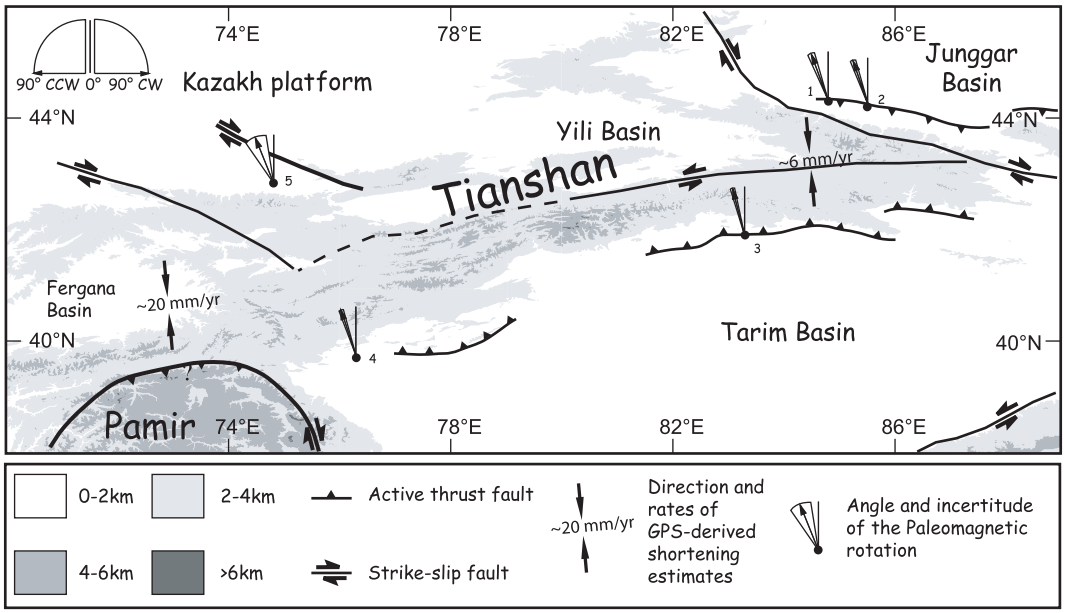

Figure 13. Simplified topographic map with site location of studies presented on Table 2 and their paleomagnetic rotations with respect to the synthetic Eurasian apparent polar wander path (APWP) [*Besse and Courtillot*, 2002]. Sources are 1, *Charreau et al.* [2005]; 2, this study; 3, *Charreau et al.* [2006]; 4, *Chen et al.* [2002]; and 5, *Bullen et al.* [2001].

is dated from the early Pleistocene up to 2.48 Ma [*Feng and Dai*, 2004; *Zhu et al.*, 2004; *Gaboardi et al.*, 2005]. The age designation stemming from this finding has had considerable impact, leading some workers to argue for a late Plio-Pleistocene acceleration in uplift of the Tian Shan [e.g., *Burchfiel et al.*, 1999] while others argue for an abrupt climate change at that time [*Zhang et al.*, 2001; *Liu et al.*, 1996]. Thus, knowing the age of the Xiyu Formation could have important consequences on our understanding of regional tectonics and climate.

[60] We define the Xiyu Formation at the point where the percentage of conglomerate exceeds ~75%, which we interpret as a shift from a braided fluviatile system (Dushanzi Formation, sedimentological units 10 and 11) toward a fan shaped fluviatile system (Xiyu Formation, sedimentological unit 12). This definition of the Xiyu formation and the criteria to define its base follow the original identification of the formation and is very close to most of similar studies surrounding the Tian Shan and the Tibetan Plateau [*Zheng et al.*, 2000; *Chen et al.*, 2002; *Scharer et al.*, 2004; *Heermance et al.*, 2007; *Sun et al.*, 2007], with the exception of *Huang et al.* [2006].

[61] Our magnetostratigraphic correlation at the Jingou River section dates the limit between the Dushanzi and the Xiyu formations at ~7.6 Ma. However, 60 km west of Jingou River, magnetostratigraphic analyses of the Kuitun and Dushanzi sections dates the base of the Xiyu Formation at 4.8 Ma and 4.2 Ma, respectively [*Charreau et al.*, 2005]. This leads to a difference of more than 3 Ma for the base of the Xiyu Formation from sections lying only 70 km apart. Structural and magnetostratigraphic data from the southern Tian Shan also suggest a diachronous deposition of the Xiyu Formation defined, with basal ages ranging from 1.2 to 2.8 Ma in sections less than ~6 km apart [*Chen et al.*, 2002; *Scharer et al.*, 2004]. Thus the magnetostratigraphy of the Jingou River section reinforces the idea that the deposition of the Xiyu Formation is likely diachronous along the strike of the Tian Shan range and probably within individual basins themselves. So, the thick conglomerate known as Xiyu should not yet be interpreted in climate or tectonic terms.

6.3. Cenozoic Paleomagnetic Rotations in the Tian Shan Piedmont

[62] Paleomagnetic data from several studies surrounding the Tian Shan offer the opportunity to better understand the Neogene deformation history of the region. From the data, we calculated the relative rotation of each locality with respect to the Eurasian synthetic apparent polar wander path [*Besse and Courtillot*, 2002] (Table 2) and plotted them in Figure 13. Because the paleomagnetic rotation pattern in the western Tian Shan may be complicated by the indentation of India at the Pamir syntaxis, our compilation begins east of 72°E.

[63] One quickly sees that all localities on both flanks of the range exhibit significant counterclockwise rotations, on the order of 15° to 20° (Figure 13). This could suggest that the entire Tian Shan range rotated with respect to Eurasia. However, Cretaceous and early Tertiary results collected at sites near to the Tian Shan Mountains show no, or only slightly clockwise rotations [*Li et al.*, 1988; *Chen et al.*, 1991, 1992; *Gilder et al.*, 2008], which could mean that these older rocks were back-rotated by 15° to 20°. But giving the orientation of shortening direction shown by GPS data

Table 2. Paleomagnetic Poles From the Jingou River Section and Other Previous Studies Carried Out on Cenozoic Sediments Across the Tian Shan and Relative Rotations of These Localities With Respect to the APWP for Eurasia[a]

Study	Area	Age (Ma)	Site						Paleopole			Rotation Locality/Europe (deg)	Reference
			n	Latitude °N	Longitude °E	D (deg)	I (deg)	α_{95} (deg)	λ_p (deg)	φ_p (deg)	dp/dm		
Kuitunhe	South Junggar	3.1–10.5	182	44.3	84.8	347.3	59.4	2.4	80.3	352.8	2.7/3.6	-18.5 ± 5.2[b]	*Charreau et al.* [2005]
Jingou He	South Junggar	~8.1–23	242	44.2	85.5	348.5	53.1	2.3	76.2	309.6	2.2/3.2	-18.3 ± 4.4[c]	This study
Yaha	North Tarim	5.2–12.6	388	41.9	83.3	353.1	43.3	1.8	72.5	284.5	1.4/2.2	-13.5 ± 4.5[d]	*Charreau et al.* [2006]
Boguzi He	North Tarim	1–3.5	258	39.7	76.3	349.4	43.3	1.9	73.0	290.9	1.5/2.4	-15.3 ± 3.7[b]	*Chen et al.* [2002]
Noruz	Chu Basin (north Tian Shan)	3–9	75	42.8	74.8	344.0	64.0	9.9	78.2	4.8	12.6	-20.9 ± 18.4[b]	*Bullen et al.* [2001]

[a]See *Besse and Courtillot* [2002]. Latitude-longitude coordinates or numbers indicate the site locations on the general map in Figure 9. D and I are the magnetic declination and inclination, respectively, at the corresponding site with α_{95} being the radius of the cone in which the mean direction lies within 95% confidence; n represents the number of samples at each site. The paleomagnetic pole were calculated using Enkin's software and then were compared to the apparent polar wander path (APWP reference poles to calculate rotations, with λ_p the latitude and ϕ_p the longitude, while dp/dm are the corresponding confidence angles. Relative rotations were calculated using the APWP reference for Europe from *Besse and Courtillot* [2002]. Magnetostratigraphic sections are treated as a single site. As the Kuitunhe and the Noruz sections span from 3.1 to 10.5 Ma and from 3 to 9 Ma, respectively, we compare their observed average directions with the 5 Ma reference pole. The Yaha section and the Jingou sections span from 5.2 to 12.3 Ma and from ~8.3 to 21.7 Ma, respectively; the declinations were compared to the APWP pole at 10 Ma and 15 Ma, respectively. The 5 Ma reference pole was used to determine the paleomagnetic rotation of the Boguzihe section [*Chen et al.*, 2002].

[b]APWP pole at 5 Ma: λ_p = 86.3°, φ_p = 178.7° and A_{95} = 2.6°.

[c]APWP pole at 10 Ma: λ_p = 85.0°, φ_p = 155.7° and A_{95} = 3.1°.

[d]APWP pole at 15 Ma: λ_p = 84.2°, φ_p = 154.9° and A_{95} = 3.2°.

[*Abdrakhmatov et al.*, 1996; *Reigber et al.*, 2001], the Tian Shan range is not only under pure compression, acting normal to the chain but undergoes some transpression as well. We thus propose that this transpression was partitioned into a strike-slip component in the piedmonts and a compressive component accommodated within the chain. Of potential interest is that the rotations from sites located on the northern Tian Shan piedmont are rotated slightly, yet within uncertainty limits, more counterclockwise than those from the south (Table 2). This could mean that the northern flank partitions a greater amount of range-parallel shear. The age of these rotations must be young, and thus rapid, because the Boguzi He sediments rotated some 18° since 1 Ma [*Chen et al.*, 2002]. We find no correlation between the magnitude of rotation and the age of the rock.

[64] Several workers have proposed that the Tian Shan formed in a transpressional tectonic regime with a combination of chain-normal compression and sinistral shear acting parallel to the chain [e.g., *Gallagher and Withjack*, 1980; *Thomas et al.*, 2002]. GPS data collected across the range suggest that deformation acts three times faster in the western Kyrgyz Tian Shan (~20 mm/a) than in the eastern Chinese Tian Shan (~6 mm/a) [*Abdrakhmatov et al.*, 1996; *Reigber et al.*, 2001]. From these data, *Reigber et al.* [2001] argued that the Tarim block rotates clockwise 1.0°/Ma with respect to stable Siberia. Moreover, balanced cross sections and Holocene shortening rates estimated from fault scarps at the piedmonts from both sides of the range led *Avouac et al.* [1993] to argue that Tarim rotated 7.0 ± 2.5° clockwise with respect to Junggar since ~15 Ma.

[65] Paleomagnetic constraints on the rotation of Tarim with respect to Junggar are ambiguous, which is largely because of a wide range in rotation magnitude from place to place. In an initial study of Cretaceous rocks, [*Chen et al.*, 1991] found an 8.6 ± 8.7° clockwise rotation. Yet no net rotation was identified in a subsequent study by the same authors [*Chen et al.*, 1992]. *Gilder et al.* [1996] found that paleomagnetic rotations recorded in Permian to Tertiary rocks surrounding the Tarim Basin were taking place in the late Cenozoic. By summing all of the paleomagnetic poles and comparing against stable Eurasia, they found a significant clockwise rotation of 9.4±6.4°. Thus, if the sum of all the localities averages out all the local deformation, and hence local rotations, then Tarim rotated clockwise with respect to Junggar. A significant clockwise rotation of 15.3 ± 6.7° was found in Miocene rocks located in the center of Tarim [*Dupont-Nivet et al.*, 2002]. These workers concluded that the rotation may have been local in nature. In sum, the paleomagnetic data from Tarim are broadly consistent with the GPS and neotectonic observations; however, we think that no single paleomagnetic study is truly representative of the block as a whole.

[66] We suggest that the Tian Shan piedmonts experienced not only compressive deformation by crustal shortening, but also a component of sinistral shear accommodated by left-lateral strike-slip faults that trend parallel to the range. Indeed, although many seismic focal plane solutions correspond to reversal mechanisms with pure north–south compression, several clearly indicate a transpressional component,

with others exhibiting pure strike-slip motion [*Nelson et al.*, 1987]. In sum, because the counterclockwise rotations occur too fast to account for a regional block rotation, and because seismic data show evidence for recent strike-slip movements, we favor the hypothesis of local rotation within the numerous piedmont structures to explain the Neogene paleomagnetic rotations.

7. Conclusion

[67] The Jingou River section provides a long and continuous series of late Cenozoic strata of the south Junggar basin, providing a good opportunity to decipher the building history of the Tian Shan mountains. Our approach was to first provide good age constrains using magnetostratigraphy, then to describe the evolution of sedimentary environments from sedimentological and rock magnetic analyses. Important environmental changes are mainly correlated with changes in sedimentation rate. Several magnetostratigraphic studies are now available around the Tian Shan, they all find acceleration in sedimentation rates, and several previous thermochronological studies also indicate uplift acceleration at the same time, meaning that the changes in sedimentation rate and sedimentary environments changes probably indicate that total sedimentary flux delivered to the basin increased, because of heightened uplift and erosion on the range.

[68] From this multidisciplinary study, together with similar magnetostratigraphic and thermochronological studies carried out around the Tian Shan, we conclude that the whole range probably grew in three major uplift pulses coupled with heightened erosion with (1) initiation of some deformation by 24–21 Ma, (2) the main phase of uplift at ~15 Ma, and (3) a later acceleration at ~11 Ma. Moreover, we show that the Xiyu Formation does not represent either a late Pliocene uplift of the range or a regional climate change because its deposition was not synchronous over the basin with different ages at different localities.

[69] Finally, from the high-resolution record of magnetic directions provided by the magnetostratigraphic analyses of the Jingou River section and other similar studies around the Tian Shan, we find that the Tian Shan piedmonts underwent transpressional deformation with rapid and recent rotation because of strike-slip faulting.

[70] **Acknowledgments.** The French program ECLIPSE, the Chinese project kzcx3-sw-147 and 973 2005CB422101, PRA (T05-02/T06-04) and ANR financed this study. We thank Guillaume Dupont-Nivet and an anonymous reviewer for their critical reviews that greatly improved the quality of the manuscript. This is IPGP contribution 2388.

References

Abdrakhmatov, K. Y., et al. (1996), Relatively recent construction of the Tien Shan inferred from GPS measurements crustal deformation rates, *Nature*, *384*, 450–453, doi:10.1038/384450a0.

Aitchison, J. C., A. M. Davis, Badengzhu, and H. Luo (2002), New constraints on the India-Asia collision: The lower Miocene Gangrinboche conglomerates, Yarlung Tsangpo suture zone, SE Tibet, *J. Asian Earth Sci.*, *21*(3), 251–263, doi:10.1016/S1367-9120(02)00037-8.

Appel, E., W. Rösler, and G. Corvinus (1991), Magnetostratigraphy of the Miocene-Pleistocene Surai Khola Siwaliks in West Nepal, *Geophys. J. Int.*, *105*, 191–198, doi:10.1111/j.1365-246X.1991.tb03455.x.

Avouac, J.-P., and P. Tapponnier (1992), Kinematic model of active deformation in central Asia, *C. R. Acad. Sci., Ser. II*, *315*, 1791–1798.

Avouac, J.-P., P. Tapponnier, P. Bai, M. You, and G. A. Wang (1993), Active thrusting and folding along the northern Tien Shan and late Cenozoic rotation of the Tarim relative to Dzungaria and Kazakhstan, *J. Geophys. Res.*, *98*, 11,791–11,808.

Besse, J., and V. Courtillot (2002), Apparent and true polar wander and the geometry of the geomagnetic field over the last 200 Myr, *J. Geophys. Res.*, *107*(B11), 2300, doi:10.1029/2000JB000050.

Bonis, L. de, G. D. Koufos, and S. Sen (1998), Ruminants (Bovidae and Tragulidae) from the middle Miocene (MN 5) of the island of Chios, Aegean sea (Greece), *Neues Jahrb. Geol. Palaeontol. Abh.*, *210*(3), 399–420.

Bullen, M. E., D. W. Burbank, J. I. Garver, and K. Y. Abdrakhmatov (2001), Late Cenozoic tectonic evolution of the northwestern Tien Shan: New age estimates for the initiation of mountain building, *Geol. Soc. Am. Bull.*, *113*, 1544–1559, doi:10.1130/0016-7606(2001)113<1544:LCTEOT>2.0.CO;2.

Bullen, M. E., D. W. Burbank, and J. I. Garver (2003), Building the northern Tien Shan: Integrated thermal, structural, and topographic constraints, *J. Geol.*, *111*, 149–165, doi:10.1086/345840.

Burchfiel, B. C., E. T. Brown, D. Qidong, J. Li, X. Feng, P. Molnar, J. Shi, Z. Wu, and H. You (1999), Crustal shortening on the margins of the Tian Shan, Xinjiang, China, *Int. Geol. Rev.*, *41*, 663–700.

Bureau of Geological and Mineral Resources of the Xinjiang Uygur Autonomous Region (BGMRX) (1993), Regional geology of Xinjiang Uygur Autonomous region, People's Republic of China Ministry of Geology and Mineral Resources, *Geol. Mem.*, *32*, 841 pp.

Burtman, V. S. (1975), Structural geology of the Variscan Tian Shan, USSR, *Am. J. Sci.*, *275-A*, 157–186.

Catlos, E. J., T. M. Harrison, C. E. Manning, M. Grove, S. M. Rai, M. S. Hubbard, and B. N. Upreti (2002), Records of the evolution of the Himalayan orogen from in situ Th-Pb ion microprobe dating of monazite: Eastern Nepal and western Garhwal, *J. Asian Earth Sci.*, *20*(5), 459–479, doi:10.1016/S1367-9120 (01)00039-6.

Charreau, J., Y. Chen, S. Gilder, S. Dominguez, J.-P. Avouac, S. Sen, D. Sun, Y. Li, and W.-M. Wang (2005), Magnetostratigraphy and rock magnetism of the Neogene Kuitunhe section (northwest China): Implications for Late Cenozoic uplift of the Tianshan mountains, *Earth Planet. Sci. Lett.*, *230*, 177–192, doi:10.1016/j.epsl.2004.11.002.

Charreau, J., S. Gilder, Y. Chen, S. Dominguez, J.-P. Avouac, S. Sen, M. Jolivet, Y. Li, and W. Wang (2006), Magnetostratigraphy of the Yaha section, Tarim Basin (China): 11 Ma acceleration in erosion and uplift of the Tian Shan mountains, *Geology*, *34*(3), 181–184, doi:10.1130/G22106.1.

Charreau, J., J. Sun, Y. Chen, S. Gilder, B. Huang, and Q. Wang (2008a), Addendum to "Late Cenozoic magnetochronology and paleoenvironmental changes in the northern foreland basin of the Tian Shan Mountains" by Jimin Sun, Qinghai Xu, and Baochun Huang, *J. Geophys. Res.*, *113*, B06103, doi:10.1029/2007JB005489.

Charreau, J., Y. Chen, S. Gilder, and L. Barrier (2008b), Comment on "Magnetostratigraphic study of the Kuche Depression, Tarim Basin, and Cenozoic uplift of the Tian Shan Range, western China" Baochun Huang, John D. A. Piper, Shoutao Peng, Tao Liu, Zhong Li, Qingchen Wang, Rixiang Zhu [*Earth Planet. Sci. Lett.,* 2006, doi:10.1016/j.epsl.2006.09.020], *Earth Planet. Sci. Lett.*, *268*, 325–329, doi:10.1016/j.epsl.2008.01.025.

Chen, G. (1988), Remarks on the Oioceros species (Bovidae, Artiodactyla, Mammalia) from the Neogene of China, *Vertebrata Palasiatica.*, *26*, 169–172.

Chen, H., X. L. Lin, K. N. Guan, and J. M. Xu (1994), Early Pleistocene deposits and its lower boundary (Q/N) in Tian Shan MT, Xinjiang region, *Quat. Sci.*, *1*, 38–47.

Chen, J., D. W. Burbank, K. M. Scharer, E. Sobel, J. Yin, C. Rubin, and R. Zhao (2002), Magnetochronology of the upper Cenozoic strata in the southwestern Chinese Tian Shan: Rates of Pleistocene folding and thrusting, *Earth Planet. Sci. Lett.*, *195*(1–2), 113–130, doi:10.1016/S0012-821X(01)00579-9.

Chen, Y., et al. (1991), Paleomagnetic study of Mesozoic continental sediments along the northern Tien Shan (China) and heterogeneous strain in central Asia, *J. Geophys. Res.*, *96*(B3), 4065–4082, doi:10.1029/90JB02699.

Chen, Y., J.-P. Cogné, and V. Courtillot (1992), New Cretaceous paleomagnetic poles from the Tarim Basin, northwestern China, *Earth Planet. Sci. Lett.*, *114*, 17–38, doi:10.1016/0012-821X(92)90149-P.

Cogné, J. P. (2003), PaleoMac: A Macintosh™ application for treating paleomagnetic data and making plate reconstructions, *Geochem. Geophys. Geosyst.*, *4(1), 1007, doi:10.1029/2001GC000227.*

Dumitru, T. A., D. Zhou, E. Z. Chang, S. A. Graham, M. S. Hendrix, E. R. Sobel, and A. R. Caroll (2001), Uplift, exhumation, and deformation in the Chinese Tian Shan, in *Paleozoic and Mesozoic Tectonic Evolution of Central Asia: From Continental Assembly To Intracontinental Deformation*, edited by M. S. Hendrix and G. A. Davis, in *Geol. Soc. Am. Mem.*, *194*, 71–99.

Dupont-Nivet, G., Z. Guo, R. F. Butler, and C. Jia (2002), Discordant paleomagnetic direction in Miocene rocks from the central Tarim Basin: Evidence for local deformation shallowing, *Earth Planet. Sci. Lett.*, *199*, 473–482, doi:10.1016/S0012-821X(02)00566-6.

England, P., and G. Houseman (1986), Finite strain calculations of continental deformation: 2. Comparison with the India-Asia collision zone, *J. Geophys. Res.*, *91*(B3), 3664–3676, doi:10.1029/JB091iB03p03664.

England, P., and P. Molnar (1997), The field of crustal velocity in Asia calculated from Quaternary rates of slip on faults, *Geophys. J. Int.*, *130*, 551–582, doi:10.1111/j.1365-246X.1997.tb01853.x.

Feng, X.-J., and W.-Q. Dai (2004), Lateral migration of fault activity in Weihe basin, *Acta Seismol. Sin.*, *17*(2), 190–199, doi:10.1007/BF02896933.

Fisher, R. A. (1953), Dispersion on a sphere, *Proc. R. Soc. London, Ser. A*, *217*, 295–302, doi:10.1098/rspa.1953.0064.

Fu, B., A. Lin, K.-I. Kano, T. Maruyama, and J. Guo (2003), Quaternary folding of the eastern Tian Shan, northwest China, *Tectonophysics*, *369*(1–2), 79–101, doi:10.1016/S0040-1951(03)00137-9.

Gaboardi, M., T. Deng, and Y. Wang (2005), Middle Pleistocene climate and habitat change at Zhoukoudian, China, from the carbon and oxygen isotopic record from herbivore tooth enamel, *Quat. Res.*, *63*(3), 329–338, doi:10.1016/j.yqres.2005.02.006.

Gabunia, L. (1973), *Fossil vertebrate fauna of Belometcheskaya*, in Russian, 138 pp., Metsniereba, Tbilissi, Georgia.

Gallagher, J. J., and M. O. Withjack (1980), Basement tectonics of China-Continental scale cataclastic flow, *AAPG Bull.*, *64*(5), 710–711.

Gentry, A. W., G. Rossner, and E. P. J. Heizmann (1999), Suborder Ruminantia, in *The Miocene Land Mammals of Europe*, edited by G. Rössner and K. Heissig, pp. 225–258, Dr. Friedrich Pfeil, Munich, Germany.

Geraads, D. (2003), Ruminants, other than Giraffidae from the middle Miocene hominoid locality of Çandir (Turkey), *Courier Forschunginst. Senckenberg*, *240*, 181–199.

Gilder, S., X. Zhao, R. Coe, Z. Meng, V. Courtillot, and J. Besse (1996), Paleomagnetism, tectonics and geology of the southern Tarim basin, northwestern China, *J. Geophys. Res.*, *101*, 22,015–22,031, doi:10.1029/96JB01647.

Gilder, S., Y. Chen, and S. Sevket (2001), Oligo-Miocene magnetostratigraphy and rock magnetism of the Xishuigou section, Subei (Gansu Province, western China) and implications for shallow inclinations in central Asia, *J. Geophys. Res.*, *106*(B12), 30,505–30,521, doi:10.1029/2001JB000325.

Gilder, S. A., J. Gomez, Y. Chen, and J.-P. Cogné (2008), A new paleogeographic configuration of the Eurasian landmass resolves a paleomagnetic paradox of the Tarim Basin (China), *Tectonics*, *27*, TC1012, doi:10.1029/2007TC002155.

Heermance, R. V., J. Chen, D. W. Burbank, and C. Wang (2007), Chronology and tectonic controls of late Tertiary deposition in the southwestern Tian Shan foreland, NW China, *Basin Res.*, *19*, 599–632, doi:10.1111/j.1365-2117.2007.00339.x.

Hendrix, M. S., A. S. Graham, A. R. Carroll, E. R. Sobel, C. L. McKnight, B. J. Schulein, and Z. Wang (1992), Sedimentary record and climatic implications of deformation in the Tian Shan: Evidence from Mesozoic strata of the north Tarim, south Junggar, and Turpan basins, northwest China, *Geol. Soc. Am. Bull.*, *104*, 53–79, doi:10.1130/0016-7606(1992)104<0053:SRACIO>2.3.CO;2.

Hendrix, M. S., T. A. Dumitru, and A. S. Graham (1994), Late Oligocene-early Miocene unroofing in the Chinese Tian Shan: An early effect of the India-Asia collision, *Geology*, *22*, 487–490, doi:10.1130/0091-7613(1994)022<0487:LOEMUI>2.3.CO;2.

Hrouda, F. (1982), Magnetic anisotropy of rocks and its application to geology and geophysics, *Geophys. Surv.*, *5*, 37–82, doi:10.1007/BF01450244.

Huang, B., J. D. A. Piper, S. Peng, T. Liu, Z. Li, Q. Wang, and R. Zhu (2006), Magnetostratigraphic study of the Kuche Depression, Tarim Basin, and Cenozoic uplift of the Tian Shan range, western China, *Earth Planet. Sci. Lett.*, *251*(3–4), 346–364, doi:10.1016/j.epsl.2006.09.020.

Jaeger, J. J., V. Courtillot, and P. Tapponnier (1989), Paleantological view of the ages of the Decan Traps, the Cretaceous/Tertiary boundary, and the India-Asia collision, *Geology*, *17*, 316–319, doi:10.1130/0091-7613(1989)017<0316:PVOTAO>2.3.CO;2.

Jelinek, V. (1981), Characterization of the magnetic fabrics of rocks, *Tectonophysics*, *79*, TT63–TT67, doi:10.1016/0040-1951(81)90110-4.

Kanamatsu, T., E. Herroro-Bervera, A. Taira, S. Saito, and J. Ashi (1996), Magnetic fabric development in tertiary accretionary complex in the Boso and Miura Peninsulas of central Japan, *Geophys. Res. Lett.*, *23*(5), 471–474, doi:10.1029/96GL00147.

Kirschvink, J. L. (1980), The least squares line and plane and the analysis of paleomagnetic data, *Geophys. J. R. Astron. Soc.*, *62*, 699–712.

Kissel, C., C. Laj, B. Lehman, L. Labyrie, and V. Bout-Roumazeilles (1997), Changes in the strength of the Iceland-Scotland overflow water in the last 200,000 years: Evidence from magnetic anisotropy analysis of core SU90-33, *Earth Planet. Sci. Lett.*, *152*(1–4), 25–36, doi:10.1016/S0012-821X(97)00146-5.

Kodama, K. P. (1997), A successful rock magnetic technique for correcting paleomagnetic inclination shallowing: Case study of the Nacimiento Formation, New Mexico, *J. Geophys. Res.*, *102*(B3), 5193–5205, doi:10.1029/96JB03833.

Köhler, M. (1987), Boviden des türkischen Miozäns (Känozoikum und Braunkohlen der Turkei. 28), *Paleontol. Evol.*, *21*, 133–246.

Kostopoulos, D. S. (2005), The Bovidae (Mammalia, Artiodactyla) from the late Miocene of Akkasdagi, Turkey, *Geodiversitas*, *27*, 747–791.

Krijgsman, W. (2003), Magnetostratigraphic dating of the Çandir fossil locality (middle Miocene, Turkey), *Courier Forschunginst. Senckenberg*, *240*, 41–49.

Lacassin, R., et al. (2004), Large-scale geometry, offset and kinematic evolution of the Karakorum fault, Tibet, *Earth Planet. Sci. Lett.*, *219*(3–4), 255–269, doi:10.1016/S0012-821X(04)00006-8.

Le Goff, M., H. Bernard, and L. Daly (1992), Practical method for drawing a VGP path, *Phys. Earth Planet. Inter.*, *70*(3–4), 201–204, doi:10.1016/0031-9201(92)90183-V.

Li, Y., Z. Zhang, M. McWilliams, R. Sharps, Y. Zhai, Y. Li, Q. Li, and A. Cox (1988), Mesozoic paleomagnetic results of the Tarim craton: Tertiary relative motion between China and Siberia?, *Geophys. Res. Lett.*, *15*, 217–220, doi:10.1029/GL015i003p00217.

Liu, T., M. Ding, and E. Derbyshire (1996), Gravel deposits on the margins of the Qinghai-Xizang plateau, and their environemental significance, *Palaeogeogr. Palaeoclimatol. Palaeoecol.*, *120*, 159–170, doi:10.1016/0031-0182(95)00039-9.

Lourens, L. J., F. J. Hilgen, J. Laskar, N. J. Shackelton, and D. S. Wilson (2004), The Neogene period, in *A Geologic Time Scale*, edited by F. M. Gradstein, J. G. Ogg, and A. G. Smith, pp. 409–440, Cambridge Univ. Press, Cambridge, U. K.

Martin-Hernandez, F., C. M. Luneburg, C. Aubourg, and M. Jackson (2004), Magnetic fabric: Methods and applications-An introduction, in *Magnetic Fabric: Methods and Applications*, edited by F. Martín-Hernández et al., *Geol. Soc. Spec. Publ.*, *238*, 1–8.

McFadden, P. L. (1990), A new fold test for palaeomagnetic studies, *Geophys. J. Int.*, *103*, 163–169, doi:10.1111/j.1365-246X.1990.tb01761.x.

McFadden, P. L., and M. W. McElhinny (1990), Classification of the reversal test in paleomagnetism, *Geophys. J. Int.*, *103*, 725–729, doi:10.1111/j.1365-246X.1990.tb05683.x.

Métivier, F., and Y. Gaudemer (1997), Mass transfer between eastern Tien Shan and adjacent basins (central Asia): Constraints on regional tectonics, *Geophys. J. Int.*, *128*, 1–17, doi:10.1111/j.1365-246X.1997.tb04068.x.

Métivier, F., Y. Gaudemer, P. Tapponnier, and K. Michel (1999), Mass accumulation rates in Asia during the Cenozoic, *Geophys. J. Int.*, *137*, 280–318, doi:10.1046/j.1365-246X.1999.00802.x.

Molnar, P. (2004), Late Cenozoic increase in accumulation rates of terrestrial sediments: How might climate change have affected erosion rates?, *Annu. Rev. Earth Planet. Sci.*, *32*, 67–89, doi:10.1146/annurev.earth.32.091003.143456.

Molnar, P., and P. England (1990), Late Cenozoic uplift of mountain ranges and global climate change: Chicken or egg?, *Nature*, *346*, 29–34, doi:10.1038/346029a0.

Molnar, P., P. England, and J. Martinod (1993), Mantle dynamics, uplift of the Tibetan Plateau, and the Indian monsoon, *Rev. Geophys.*, *31*(4), 357–396, doi:10.1029/93RG02030.

Molnar, P., et al. (1994), Quaternary climate change and the formation of river terraces across growing anticlines on the north flank of the Tien Shan, China, *J. Geol.*, *102*, 583–602.

Nelson, M. R., R. McCaffrey, and P. Molnar (1987), Source parameters for 11 earthquakes in the Tian Shan, central Asia, determined by P and Sh waveform inversion, *J. Geophys. Res.*, *92*(B12), 12,629–12,648, doi:10.1029/JB092iB12p12629.

Opdyke, N. D., E. Lindsay, N. Johnson, R. A. K. Tahirkheli, and M. A. Mirza (1979), Magnetic polarity stratigraphy and vertebrate paleontology of the upper Siwalik subgroup of northern Pakistan, *Palaeogeogr. Palaeoclimatol. Palaeoecol.*, *27*, 1–34, doi:10.1016/0031-0182(79)90091-9.

Parès, J. M., and B. Van der Pluijm (2002), Evaluating magnetic lineations (AMS) in deformed rocks, *Tectonophysics*, *350*, 283–298, doi:10.1016/S0040-1951(02)00119-1.

Patriat, P. A., and J. Achache (1984), India-Eurasia collision chronology has implications for crustal shortening and driving mechanisms of plates, *Nature*, *311, 615–621, doi:10.1038/311615a0.*

Peltzer, G., P. Tapponnier, and P. Cabbold (1982), Les grands décrochements de l'Est asiatique, évolution dans le temps et comparaison avec un modèle expérimental, *C. R. Acad. Sci., Ser. 2*, *294*, 1341–1348.

Pilgrim, G. E. (1934), Two new species of sheep-like antelope from the Miocene of Mongolia, *Am. Mus. Novit.*, *716*, 1–29.

Poisson, B., and J.-P. Avouac (2004), Holocene hydrological changes inferred from alluvial stream entrenchment in north Tian Shan (northwestern China), *J. Geol.*, *112*, 231–249, doi:10.1086/381659.

Rage, J. C., et al. (1995), Collision age, discussion, *Nature*, *375*, 286, doi:10.1038/375286c0.

Reigber, C., G. W. Michel, R. Galas, D. Angermann, J. Klotz, J. Y. Chen, A. Papschev, R. Arslanov, V. E. Tzurkov, and M. C. Ishanov (2001), New space geodetic constraints on the distribution of deformation in the central Asia, *Earth Planet. Sci. Lett.*, *191*, 157–165, doi:10.1016/S0012-821X(01)00414-9.

Roberts, A. P., and M. Winklhofer (2004), Why are geomagnetic excursions not always recorded in sediments? Constraints from post-depositional remanent magnetization lock-in modelling, *Earth Planet. Sci. Lett.*, *227*(3–4), 345–359, doi:10.1016/j.epsl.2004.07.040.

Robion, P., S. Grelaud, and D. Frizon de Lamotte (2007), Pre-folding magnetic fabrics in fold-and-thrust belts: Why the apparent internal deformation of the sedimentary rocks from the Minervois basin (NE-Pyrenees, France) is so high compared to the Potwar basin (SW-Himalaya, Pakistan)?, *Sediment. Geol.*, *196*, 181–200, doi:10.1016/j.sedgeo.2006.08.007.

Scharer, K. M., D. W. Burbank, J. Chen, R. J. Weldon, C. Rubin, R. Zhao, and J. Shen (2004), Detachment folding in the southwestern Tian Shan-Tarim foreland, China: Shortening estimates and rates, *J. Struct. Geol.*, *26*, 2119–2137, doi:10.1016/j.jsg.2004.02.016.

Sobel, E. R., M. Oskin, D. Burbank, and A. Mikolaichuk (2006), Exhumation of basement-cored uplifts: Ex-

ample of the Kyrgyz Range quantified with apatite fission track thermochronology, *Tectonics*, *25*, TC2008, doi:10.1029/2005TC001809.

Sokolov, J. J. (1949), On the remains of Cavicornia (Bovidae, Mammalia) from the middle Miocene of the North Caucasus, *Dokl. Akad. Nauk SSSR*, *67*(6), 1101 – 1104.

Sun, J. (2004), Timing of the Tianshan Mountains uplift constrained by magnetostratigraphic analysis of molasse deposits, *Earth Planet. Sci. Lett.*, *219*, 239 – 253, doi:10.1016/S0012-821X(04)00008-1.

Sun, J., Q. Xu, and B. Huang (2007), Late Cenozoic magnetochronology and paleoenvironmental changes in the northern foreland basin of the Tian Shan Mountains, *J. Geophys. Res.*, *112*, B04107, doi:10.1029/2006JB004653.

Tapponnier, P., and P. Molnar (1976), Slip-line field theory and large-scale continental tectonics, *Nature*, *264(5584), 319 – 324, doi:10.1038/264319a0.*

Tapponnier, P., R. Lacassin, H. Leloup, U. Schärer, D. Zhong, H. Wu, X. Liu, S. Ji, L. Zhang, and J. Zhong (1990), The Ailao Shan/Red River metamorphic belt: Tertiary left-lateral shear between Indochina and south China, *Nature*, *343*(6257), 431 – 437, doi:10.1038/343431a0.

Tapponnier, P., Z. Xu, F. Roger, B. Meyer, N. Arnaud, G. Wiltinger, and J. Yang (2001), Oblique stepwise rise and growth of the Tibet Plateau, *Science*, *294*, 1671 – 1677, doi:10.1126/science.105978.

Thomas, J. C., R. Lanza, A. Kazansky, V. Zykin, N. Semakov, D. Mitrokhlin, and D. Delavaux (2002), Paleomagnetic study of Cenozoic sediments from the Zaisan basin (SE Kazakhstan) and the Chuya depression (Siberian Altai): Tectonic implications for central Asia, *Tectonophysics*, *351*, 119 – 137, doi:10.1016/S0040-1951(02)00128-2.

Wang, X., Z. Qui, and N. D. Opdyke (2003), Litho-, bio-, and magnetostratigraphy and paleoenvironment of Tunggur Formation (middle Miocene) in central inner Mongolia, China, *Am. Mus. Novit.*, *3411*, 1 – 31, doi: 10.1206/0003-0082(2003)411<0001:LBAMAP>2.0.CO;2.

Windley, B. F., M. B. Allen, C. Zhang, Z.-Y. Zhao, and G. R. Wang (1990), Paleozoic accretion and Cenozoic deformation of the Chinese Tien Shan Range, central Asia, *Geology*, *18*, 128 – 131, doi:10.1130/0091-7613(1990)018<0128:PAACRO>2.3.CO;2.

Zhang, P., P. Molnar, and W. R. Downs (2001), Increased sedimentation rates and grain sizes 2 – 4 Myr ago due to the influence of climate change on erosion rates, *Nature*, *410*, 891 – 897, doi:10.1038/35073504.

Zheng, H., C. M. Powell, Z. An, J. Zhou, and G. Dong (2000), Pliocene uplift of the northern Tibetan Plateau, *Geology*, *28*, 715 – 718, doi:10.1130/0091-7613(2000)28<715:PUOTNT>2.0.CO;2.

Zhu, R. X., et al. (2004), New evidence on the earliest human presence at high northern latitudes in northeast Asia, *Nature*, *431*, 559 – 561, doi:10.1038/nature02829.

Zijderveld, J. D. A. (1967), A. C. demagnetization of rocks: Analysis of results, in *Methods in Paleomagnetism*, edited by D. W. Collinson, K. M. Creer, and S. K. Runcorn, pp. 254 – 286, Elsevier, Amsterdam, Netherlands.

R. Augier, Y. Chen, and A. Gallaud, Institut des Sciences de la Terre d'Orléans, Bâtiment Géosciences, rue de Saint Amand, BP 6759, F-45067 Orléans CEDEX 2, France. (Romain.augier@univ-orleans.fr; Yan.Chen@univ-orleans.fr)

J.-P. Avouac, Tectonics Observatory, California Institute of Technology, Mail Code 100-23, Pasadena, CA 91125, USA. (avouac@gps.caltech.edu)

L. Barrier, Institut de Physique du Globe de Paris, 4 place Jussieu, F-75252 Paris CEDEX 05, France. (barrier@ipgp.jussieu.fr)

J. Charreau, Centre de Recherches Petrographiques et Geochimiques, 15, rue Notre Dame des Pauvres, F-54500 Vandoeuvre-lès-Nancy, France. (charreau@crpg.cnrs-nancy.fr)

S. Dominguez and F. Graveleau, Géosciences Montpellier, UMR 5243, UMII, cc.60, Université Montpellier 2, CNRS, F-34095 Montpellier CEDEX, France. (dominguez@dstu.univ-montp2.fr; fabien.graveleau@gm.univ-montp2.fr)

S. Gilder, Geophysics Section, Department of Earth and Environmental Sciences, Ludwig Maximilians University, Theresienstrasse 41, D-80333 Munich, Germany. (gilder@geophysik.uni-muenchen.de)

S. Sen, Museum of Natural History, UMR 5143, Paléobiodiversité et Paléoenvironnements, CNRS, 8 rue Buffon, F-75005 Paris CEDEX 5, France. (sen@mnhn.fr)

Q. Wang, State Key Laboratory of Lithospheric Evolution, Institute of Geology and Geophysics, Chinese Academy of Sciences, Beijing 100029, China. (qcwang@mail.igcas.ac.cn)